BAMS Article

A Multiagency Experiment on Internal Wave Energy, Mixing, and Interactions and Their Representation in Global Ocean Models and Operational Forecasts

Maarten C. Buijsman,[a] Amy F. Waterhouse,[b] Edward D. Zaron,[c] Badarvada Yadidya,[d] Chengzhu Xu,[c] Victoria Whitley,[e] Jacob O. Wenegrat,[e] Jinbo Wang,[f] Alan J. Wallcraft,[g] Dheeraj Varma,[a] Babette C. Tchonang,[g] Oladeji Siyanbola,[a] Jay F. Shriver,[i] Vitalii A. Sheremet,[j] Uwe Send,[b] Keshav J. Raja,[g] Kurt Polzin,[j] Hans E. Ngodock,[i] Aurelie J. Moulin,[k] Grant Meiners,[b] Andrew J. Lucas,[b,l] Matthias Lankhorst,[b] Joseph J. Kuehl,[m] Samuel M. Kelly,[n] Luke Kachelein,[h] Yonglin Huang,[o] Caeli Griffin,[b] James B. Girton,[k] J. Thomas Farrar,[j] Audrey Delpech,[h] Zihan Chen,[e] Eric P. Chassignet,[g] Matthew J. Carrier,[i] Annalisa Bracco,[o,p] Brian K. Arbic,[d] Magdalena Andres,[j] and Mujeeb A. Abdulfatai[a]

KEYWORDS: Internal waves; Wave breaking; Boundary layer; In situ oceanic observations; Satellite observations; Ocean models

ABSTRACT: As part of a National Oceanographic Partnership Program (NOPP) project, seven teams—comprising investigators from universities, federal laboratories, and industry—are collaboratively investigating the generation, propagation, and dissipation of internal waves in the global ocean using complementary, state-of-the-art observations and model simulations. Internal waves, generated by the interaction of tides, winds, and mean flows, permeate the ocean and influence its physical state. Internal waves transport scalar and vector properties—both geographically and across scales—and contribute to irreversible mixing, modulate acoustic propagation, and complicate the identification of subinertial (e.g., geostrophic) flows in observations. For these reasons, accurately representing internal waves in global ocean forecast models is a high priority. The collaborations reported here are improving the understanding of the internal wave life cycle and enhancing model skill in simulating it. Three observational teams are collecting in situ data using 1) redeployable moored arrays that resolve internal waves from multiple directions, 2) global deployments of profiling floats that measure internal wave energy fluxes, shear, and mixing, and 3) high-resolution arrays that focus on bottom boundary layer processes. Four modeling teams are guiding the design and placement of these observation platforms and are using the collected observations to 1) improve internal wave representation and dissipation in ocean models, 2) conduct high-resolution process studies, and 3) implement data assimilation in idealized, regional, and global simulations. These efforts are further supported by high-resolution sea surface height measurements from the new Surface Water and Ocean Topography (SWOT) satellite, which provide context for in situ observations and improve ocean forecasting systems.

DOI: 10.1175/BAMS-D-24-0174.1

Corresponding author: Maarten C. Buijsman, maarten.buijsman@usm.edu

Manuscript received 20 June 2024, in final form 17 November 2025, accepted 6 December 2025

SIGNIFICANCE STATEMENT: A collaboration among scientists from U.S. universities, national laboratories, and industry is advancing our understanding and prediction of internal waves in the global ocean. These waves—characterized by vertical scales of tens to hundreds of meters and horizontal scales of tens to hundreds of kilometers—play a critical role in maritime commerce, naval operations, and ocean circulation. The team integrates novel observational approaches, including internal wave–resolving moored arrays, ship-of-opportunity float deployments, bottom boundary layer–distributed sensor networks, and satellite wide-swath altimetry, with cutting-edge global, regional, and process-model simulations. Together, these efforts are improving the representation of internal wave processes in ocean models and enhancing their predictive capabilities for operational forecasts.

AFFILIATIONS: [a] University of Southern Mississippi, Stennis Space Center, Mississippi; [b] Scripps Institution of Oceanography, University of California San Diego, La Jolla, California; [c] Oregon State University, Corvallis, Oregon; [d] University of Michigan, Ann Arbor, Michigan; [e] University of Maryland, College Park, College Park, Maryland; [f] Texas A&M University, College Station, Texas; [g] Florida State University, Tallahassee, Florida; [h] Jet Propulsion Laboratory, California Institute of Technology, Pasadena, California; [i] U.S. Naval Research Laboratory, Stennis Space Center, Mississippi; [j] Woods Hole Oceanographic Institution, Woods Hole, Massachusetts; [k] Applied Physics Laboratory, University of Washington, Seattle, Washington; [l] Department of Mechanical and Aerospace Engineering, University of California San Diego, La Jolla, California; [m] University of Delaware, Newark, Delaware; [n] University of Minnesota Duluth, Duluth, Minnesota; [o] Georgia Institute of Technology, Atlanta, Georgia; [p] The CMCC Foundation (Euro-Mediterranean Center on Climate Change), Milano, Italy

1. Introduction

Analogous to surface gravity waves that occur at the interface between air and water, internal gravity waves exist at the interface between lighter and denser water layers in the ocean interior. Unlike surface gravity waves, which have amplitudes of meters, wavelengths of tens of meters, and periods of seconds, the largest internal waves have amplitudes of 100 m or more, wavelengths of hundreds of kilometers, and periods of hours (e.g., Gill 1982). Since the first recorded measurements of internal waves in 1893 (Nansen 1897), their life cycle has been a topic of active research because internal waves provide a fundamental conduit by which energy is input into the global ocean. This can occur either via direct forcing by winds or tides, or indirectly through exchange with subinertial flows. Energy eventually cascades to smaller scales, and it has been hypothesized that internal wave breaking is the rate-limiting step for the turbulent mixing that plays a role in sustaining the meridional overturning circulation (Munk and Wunsch 1998; MacKinnon et al. 2017; Melet et al. 2016; Buijsman et al. 2019). More broadly, internal waves are fundamental partners with subinertial flows in closing oceanic mass, momentum, energy, and potential vorticity budgets.

Though internal waves' expression on the sea surface is subtle, they strongly influence many aspects of ocean processes and maritime commerce and operations. Wind- and tidally generated internal waves, known as near-inertial waves and internal tides, respectively, can travel thousands of kilometers across ocean basins (Fig. 1; Dushaw et al. 1995; Ray and Mitchum 1996; Zhao et al. 2016; Buijsman et al. 2025; Raja et al. 2022) increasing internal wave energy levels and mixing along the continental margins (Kelly et al. 2013; Siyanbola

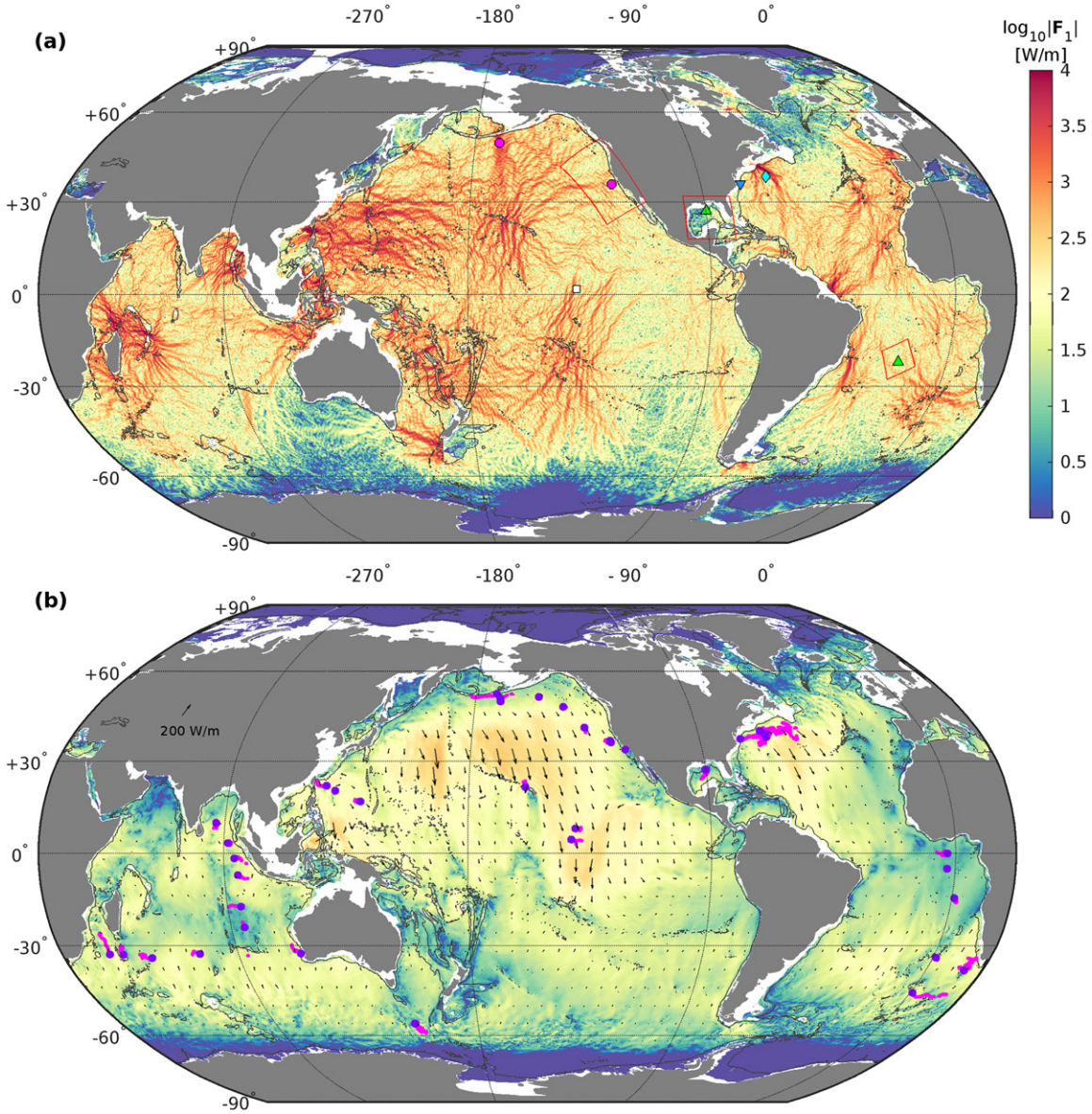

FIG. 1. The M_2 mode-1 internal tide energy flux radiates from ridges and shelves in (a), while the wind-generated near-inertial mode-1 energy flux is directed equatorward from the midlatitudes in (b). Fields in (a) are extracted from a 1/25° HYCOM (Bleck 2002) simulation (Buijsman et al. 2020) and time averaged over the first 2 weeks of September 2016. Fields in (b) are extracted from a 1/12.5° HYCOM simulation (Buijsman et al. 2020) and time averaged over a year from October 2011 to September 2012. In (a), regional model simulation boundaries are marked by the red curves (Figs. 10, 12, and 13). The colored symbols represent the following NOPP GIW observations: IWR Arrays (magenta circles; Figs. 2 and 3), the Distributed Sensor Network (green triangles; Fig. 6), and EM-APEX float tracks [magenta dots in (b) with the deployment locations shown with dark purple dots; Fig. 5]. As part of NOPP GIW, CPIESs have been added to other project arrays: Mixing Below Tropical Instability Waves (MOTIVE; white square), Task Force Ocean New England Seamount Acoustics Experiment (TFO/NESMA; cyan diamond), and the Mid-Atlantic Bight (MAB)-SWOT crossover (blue upside-down triangle).

et al. 2023, 2024), with detection even in the surf zone (Kumar et al. 2021). As they cascade to smaller scales, breaking internal waves drive diapycnal mixing that disperses heat, nutrients, and sediments (e.g., Lucas et al. 2011; Villamaña et al. 2017; Boegman and Stastna 2019; Zulberti et al. 2020). Energetic internal waves impact the transmission of acoustic signals (e.g., Little 1966; Headrick et al. 2000; Lynch et al. 2010; Colosi 2016; Hiron et al. 2025; Schönau et al. 2025) and underwater vessel navigation (e.g., Little 1966; Neuman 2021; Chen et al. 2022). Hence, it is important to predict their occurrence, energy, and phase, for example, with hydrodynamic and/or altimetry-constrained models (Zaron 2019; Yadidya et al. 2024).

Two thematic lines of research on internal waves have emerged that suggest a surface wave analogy, in which the wave field is recognized as being composed of two parts. The first, the wind wave field, relates to the local wind. The wind wave analogy for internal waves is generally quantified with spectral representations introduced in Garrett and Munk (1975). The second analogy is with swell, which is quasi deterministic and related to distant generation associated with storms (Alford 2001) or tide-topography interactions. Internal swell is those waves with the largest group velocities, limited to the lowest vertical modes, that minimally interact with other waves and subinertial flows.

Early modern day[1] research on internal waves was largely guided by the wind wavefield framework and thus developed observational tools that were good at shorter space and time scales and a theoretical focus on explaining the possibility of a "universal" spectrum (Briscoe 1975; Wunsch and Ferrari 2004; Garrett and Munk 1979; Munk 1981; Müller et al. 1986). This line of investigation provided a direct link to mixing but not to the regional variability set up by the patterns of larger-scale forcing. In the post-1993 satellite altimetry era, regional patterns of the internal wave field could be identified from observations of ocean surface height as long-wavelength internal waves at tidal frequencies (Ray and Mitchum 1996; Carrère et al. 2021). Altimetry also provided the first reliable estimate for the generation rate of internal waves by tides at large-scale topographic features in the deep ocean (Egbert and Ray 2000), thus making a quantitative link to the mechanical energy budget of the global ocean. Polzin and Lvov (2011) found that if one averages energy spectra over multiple eddy time scales, regional variability in the parametric spectral fits, i.e., the wind wave analogy, exists. They further hypothesized that this regional variability can be understood in terms of variability in the major sources, mesoscale flows, and major nonlinear transfer mechanisms, thus pointing toward dynamical linkages between internal swell and the wind wave analogy.

[1] Polzin and McDougall (2022) locate the dawn of modern oceanography with the development of near-continuously profiling instrumentation in the early 1970s.

Additional insights into the spatiotemporal global internal field were obtained when tidal forcing (e.g., Niwa and Hibiya 2001; Arbic et al. 2004; Simmons et al. 2004) and both tidal and high-frequency wind forcing (e.g., Arbic et al. 2010; Müller et al. 2012; Simmons and Alford 2012; Jochum et al. 2013) were incorporated into global circulation models. The continuous development of these realistically forced global ocean models, including efforts by the NSF-funded Climate Process Team (MacKinnon et al. 2017), has enhanced our capacity to investigate ocean internal waves and how their parameterized effects modify ocean forecasting (Melet et al. 2013a,b, 2014, 2015, 2016). Several developments have contributed to this. Foremost, the continued increase in computational power has facilitated the increase of grid resolutions that resolve smaller-scale internal waves. As a consequence, these global ocean simulations have begun to resolve the internal gravity wave continuum spectrum (Müller et al. 2015; Rocha et al. 2016; Savage et al. 2017; Arbic et al. 2018). The accuracy of surface tides, and thus tidally generated internal waves, has improved with the inclusion of a spatially varying self-attraction and loading (SAL) term in conjunction with a Kalman filter (Ngodock et al. 2016) and linear wave drag formulations that dampen the surface and internal tides (e.g., Arbic et al. 2004; Buijsman et al. 2015; Xu and Zaron 2025). The accuracy of the internal tides, in phase and amplitude, has also improved due to data assimilation (DA), which ensures the background flow is simulated more realistically (e.g., Luecke et al. 2017; Yadidya et al. 2024). Finally, the improvement of the fidelity of wind-generated near-inertial waves in global ocean simulations is attributed to increases in model resolution and wind forcing frequency, the type of wind product used, and two-way atmosphere–ocean coupling (e.g., Furuichi et al. 2008; Simmons and Alford 2012; Flexas et al. 2019; Raja et al. 2022; Sun et al. 2024). Because of the improved realism of the global ocean simulations, we can now use their fields as the boundary conditions for regional numerical simulations (e.g., Nelson et al. 2020;

Siyanbola et al. 2023; Skitka et al. 2024a,b). These regional simulations can provide diagnostics about the aforementioned hypothetical linkages between internal "swell" and internal "wind" waves that can justify regional patterns of mixing as inferred from observations presented in Whalen et al. (2012) and Waterhouse et al. (2014). Nonetheless, substantial challenges remain in improving model representations of internal waves and energy dissipation pathways. Ongoing validation against high-resolution in situ and satellite observations is critical for constraining model uncertainties and guiding future developments.

We are a large team of academic, federal, and industry partners that is collaborating to substantially advance our knowledge on internal waves as part of a National Oceanographic Partnership Program (NOPP) Global Internal Waves (GIW) project "A Global Multi-Agency Experiment on Internal Wave Energy, Mixing, and Interactions in the Ocean and their Representation in Global Ocean Models and Operational Forecasts." We bring a diverse expertise across a broad range of tools and physical processes connected with internal waves, and we are motivated by improving the representation of internal waves in numerical models. Our team has been coordinating large observational field programs, designed to cover vast ranges of temporal and spatial scales across the global ocean basins (Fig. 1). By leveraging in situ instrumentation, remote sensing data, and numerical models, we aim to address the following research questions in our NOPP project:

1) What are the primary processes by which internal waves dissipate, how do these processes vary across scales, and what are the implications for ocean mixing?
2) Do model simulations capture the internal wave life cycle with enough fidelity to provide realistic estimates of the propagation and arrival of both tidal and broadband internal wave energy?
3) How do the observed internal waves compare with the global model predictions in terms of intensity, variability, and modal structure?

In this paper, we highlight recent developments, enabled by this NOPP GIW, in observing and simulating internal waves. These developments are broadly categorized as follows: 1) instrumentation and array design and 2) model improvement and validation using observations, with the goal to improve our understanding of the internal wave life cycle from generation to dissipation. In the remainder of this paper, we present advances in internal wave observations and simulations in section 2. We conclude with a discussion on future developments and synergies in section 3.

2. Methods and results

a. Observational techniques. The NOPP GIW observations serve a dual purpose: 1) understanding internal wave processes and 2) the validation of (global) ocean model simulations. In this section, we discuss an Internal Wave Resolving (IWR) Array, coincident Surface Water and Ocean Topography (SWOT) observations, velocity and turbulence profiling floats, and a distributed sensor network.

1) Internal wave resolving array. Unlike a single point mooring, which can only detect the average amplitude and direction for each frequency of the broadband internal wave field, the IWR Array was designed to detect multiple internal tide beams simultaneously. The array combines a central mooring to resolve the waves' modal structure surrounded by an antenna of acoustic instruments to provide vertically integrated measures of the speed and direction of internal wave propagation. Before each deployment, coordination with the NOPP GIW modeling teams allowed for the optimization of the central mooring and antenna spacing (Figs. 2d–f).

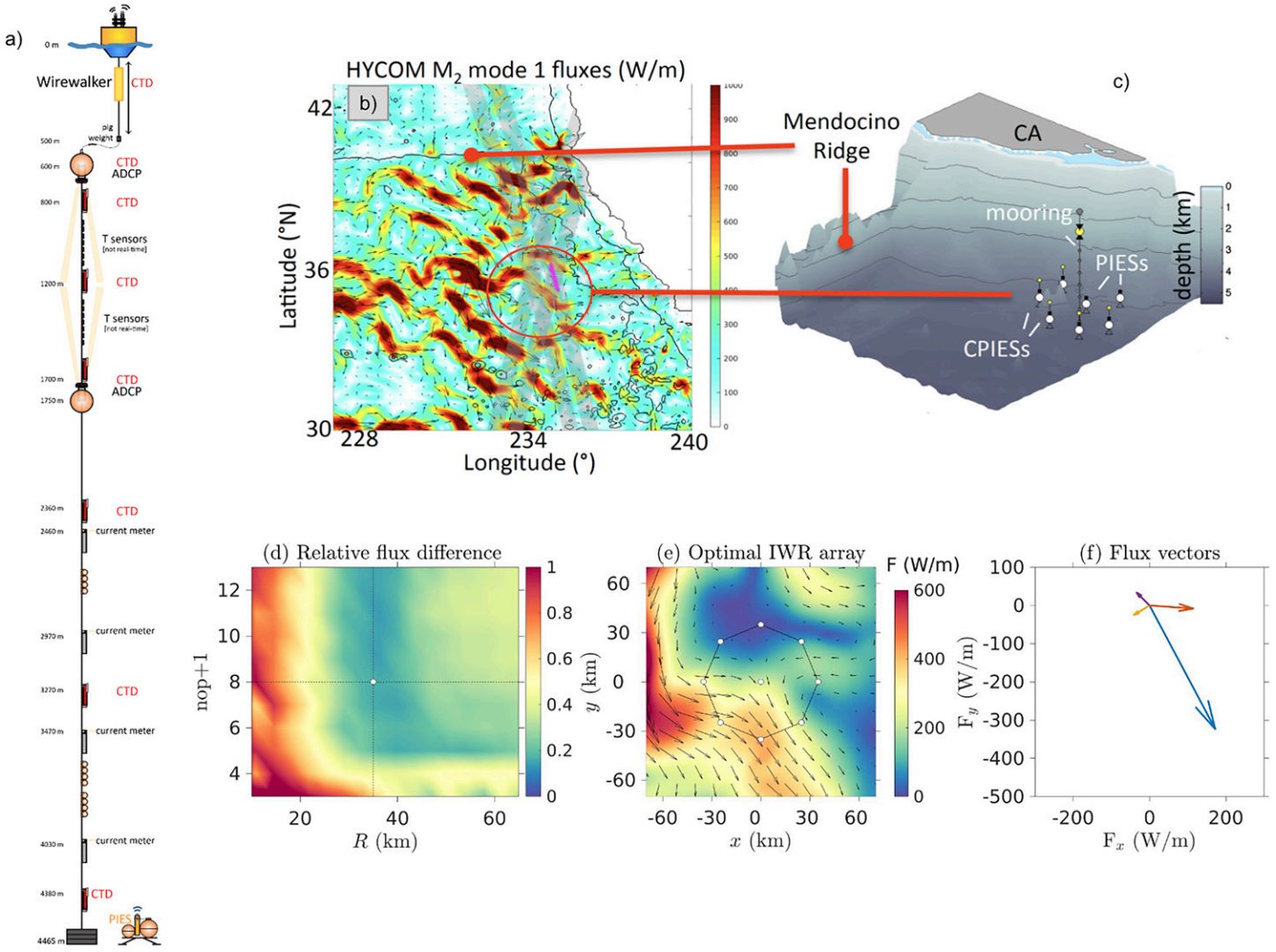

FIG. 2. Schematics for the first IWR Array deployment during the 2023 SWOT Cal/Val. (a) SIO hybrid CTD–velocity–Wirewalker–dynamic height mooring [SIO hybrid mooring; Wang et al. (2022); Schematic courtesy of Jeffrey Sevadjian, SIO], consisting of a surface buoy, profiling Wirewalker in the upper 500 m (with a Nortek Signature 1000 kHz ADCP, RBR CTD, and real-time telemetry). A taut subsurface mooring (600–4500-m depth) was coupled to the surface buoy and Wirewalker via a catenary. The taut section of the mooring was instrumented with a series of current meters (Long Range 75-kHz ADCPs and Nortek Aquadopps), SBE37 CTDs, and RBR SoloTs. (b) As part of the predeployment planning, the modeled mode-1 semidiurnal (M_2) energy flux from a global 1/25° HYCOM simulation (Buijsman et al. 2020) was used to guide the IWR Array placement. The NASA SWOT Cal/Val sites are marked with magenta crosses (Wang et al. 2025). (c) Schematic of the deployed IWR Array consisting of the SIO hybrid mooring surrounded by CPIESs (location of the continental slope is exaggerated). (d) A Multivariable Plane (MVARP) wave fit technique (Varma et al. 2026) is applied to HYCOM mode-1 M_2 horizontal velocity and pressure fields to design the most optimal IWR Array configuration that allows for the measurement of mode-1 M_2 internal waves from multiple directions. The relative vector difference between the sum of four-largest M_2 mode-1 unidirectional energy flux vectors computed with MVARP and the undecomposed mode-1 fluxes is plotted as a function of array radius (R) and the number of CPIESs (nop) on a circular IWR array. (e) The optimal array configuration, overlaid on the M_2 mode-1 flux of HYCOM, has the lowest error for $R \approx 35$ km and nop ≈ 8 and is marked by the white dot in (d). (f) The four-largest unidirectional mode-1 internal wave flux vectors obtained with MVARP at the central mooring location.

The IWR Array was first deployed off the coast of California at 35° 55.02′N, 125° 02.64′W, coinciding with the NASA/JPL SWOT Calibration/Validation (Cal/Val) program (Wang et al. 2025). This location was chosen for the NOPP GIW program because it features variable tidal internal wave energy fluxes generated remotely, e.g., from Hawai'i, and locally from the Mendocino Escarpment and shelf break (Figs. 1a and 2b). The IWR Array (Fig. 2c) comprised eight current- and pressure-sensor-equipped inverted echo sounders (CPIESs) in a 70-km-diameter circle surrounding a densely instrumented, full-depth hybrid CTD–velocity–Wirewalker–dynamic

height mooring [Scripps Institution of Oceanography (SIO) hybrid mooring]. An additional PIES (i.e., a CPIES without the current sensor) was collocated with the central mooring.

The central hybrid mooring of the IWR Array measured the full-depth vertical structure of temperature, salinity, and velocity for 20 months (Fig. 3) using a new design that was originally developed to obtain full-water column measurements for the NASA SWOT Cal/Val mission (Wang et al. 2022, 2025). It is a "hybrid" mooring due to the novel combination of an upper-water-column Wirewalker profiler (Pinkel et al. 2011) and a subsurface mooring section consisting of CTD sensors, multiple thermistors, current meters, and two long-range (75 kHz) acoustic Doppler current profilers (ADCPs; Tchonang et al. 2026; Fig. 2a). On average, a vertical profile of the upper 500 m with 1-m vertical resolution was collected every 30 min by the Wirewalker, which equates to more than 25,000 500-m profiles over the length of the IWR deployment. The combination of velocity and density observations allowed the behavior of the full-ocean-depth internal wave field to be quantitatively examined across frequencies spanning the inertial frequency (f) to the buoyancy frequency (N) (Fig. 3). This "top to bottom, f to N" characterization of the internal wave field for more than 600 days is a first for an open-ocean mooring. During this deployment, the mooring telemetered real-time observations to a web-based server at SIO/University of California, San Diego (UCSD)

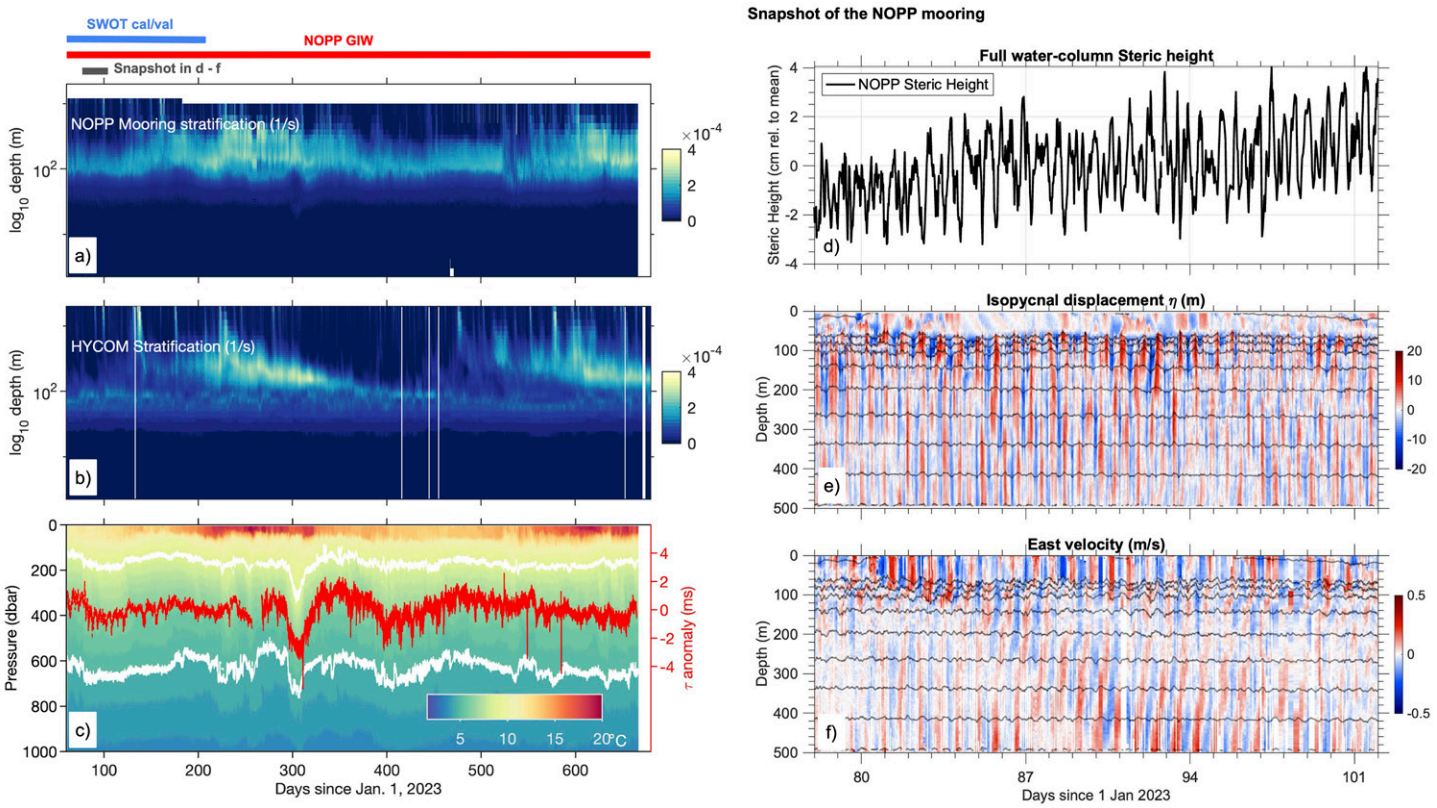

FIG. 3. Observations collected over the 20 month IWR Array deployment (SWOT 2024b; Andres 2025), coordinated with the NASA SWOT Cal/Val program. The duration of each program is noted by the blue (SWOT Cal/Val) and red (NOPP GIW) overbars in (a). (a) Observed stratification, plotted in log(depth), shows the variability of the upper-ocean stratification, some of which is captured by (b) stratification from a 1/25° HYCOM simulation during the same time period. (c) Hourly temperature profiles in the upper 1000 m from the central IWR mooring (left y axis; shading) with the 5° and 9°C isotherms highlighted in white. Hourly τ anomaly from nearby CPIESs is superimposed (right y axis; red line). Mesoscale variability results in isotherm displacements of up to 170 dbar that correspond to ~20 m s^{-1} τ anomalies, while the semidiurnal internal tide causes 1 m s^{-1} τ anomalies that correspond to ~20-dbar isotherm displacements. (right) A 3-week-long snapshot from the central IWR mooring for yeardays 78–102 (mid-March–mid-April 2023), including (d) the full-depth steric height from the NOPP GIW central IWR mooring. This mooring also includes high-resolution measurements in the upper 500 m of (e) vertical isopycnal displacements, and (f) zonal velocity (positive eastward), highlighting the ability of the hybrid mooring to observe internal waves.

(mooring.ucsd.edu). The adjacent central PIES was outfitted with an acoustic modem (modem-PIES) and also returned real-time data.

The spacing of the CPIESs distributed in a circle around the central site was chosen based on the capability of the IWR Array to resolve waves from multiple directions (Figs. 2d–f). The CPIESs measured round-trip surface-to-bottom acoustic travel time (τ), bottom pressure and temperature, and near-bottom currents at 50 m above the seabed.

Observations from the 20-month deployment illustrate the seasonal variability of stratification, particularly in the upper ocean (Fig. 3a). While the modeled stratification captures some of the observed variability, there are many high-frequency events that were not captured in the model (Fig. 3b). The high-resolution profiling (in both depth and time) of the Wirewalker in the upper 500 m of the central mooring provided a detailed view of temperature, steric height, isopycnal displacement, and velocity (Figs. 3c–f). In a 3-week-long snapshot, the hybrid mooring captured both the semidiurnal tidal variability along with an event-scale near-inertial wave event. The CPIESs detected τ anomalies associated with the internal tide's displacement of the isotherms (Fig. 3c), superimposed on the region's mesoscale variability.

2) Surface water and ocean topography mission. While regional field campaigns provide detailed observations at single locations, studying internal waves and tides globally requires remote sensing (Ray and Mitchum 1996; Carrère et al. 2021). As propagating internal waves displace and deform the thermocline, they induce steric changes in the upper ocean, manifesting as variations in sea surface height (SSH; Fig. 3d). Over the past three decades, nadir altimeters have successfully mapped coherent, mode-1, long-wavelength internal tides phase locked to tidal forcing. However, incoherent internal tides and smaller-scale nonlinear internal gravity waves remain unmapped due to spatial and temporal gaps in the nadir altimeter tracks. The joint NASA–CNES SWOT mission, launched on 16 December 2022, transforms global studies by resolving smaller wavelengths, including higher vertical modes, using its Ka-band interferometer (KaRIn; Wang et al. 2025). KaRIn resolves kilometer-scale SSH structures across a 120-km swath, enabling studies of small-scale linear and nonlinear internal waves (e.g., Qiu et al. 2024; Archer et al. 2025). Such small-scale waves, i.e., long-crested solitons, can be observed in both SWOT and a 1/50° HYCOM simulation in Fig. 4. However, the simulation underresolves the abundance of small-scale features seen in SWOT. Leveraging SWOT's rich observational information to enhance modeling remains an area of active research.

3) Velocity and turbulence profiling floats (SQUID). To permit characterization of a broad range of oceanic internal wave environments and facilitate the validation of internal wave–resolving models across ocean basins, we are deploying autonomous profiling floats (Fig. 5a) measuring temperature, salinity, horizontal currents, and turbulent mixing from cruises of opportunity. The floats [electromagnetic autonomous profiling explorer (EM-APEX); Sanford et al. 2005] are similar to those used in the global Argo array but with the addition of electrodes sensing the conducting seawater's motion (Fig. 5b) in the geomagnetic field (Sanford 1971), as well as fast-response FP07 thermistors to measure the rate of temperature gradient dissipation by turbulence (Fig. 5d; Lien et al. 2016). This component of NOPP GIW is denoted Sampling Quantitative Internal-Wave Distributions ("SQUID") and aims to span the broad range of internal wave environments, forcing, and propagation parameters (e.g., wind, tide, mesoscale eddies, water depth, topographic roughness, stratification, and latitude).

The initial deployment phase consists of 50 floats distributed globally (Fig. 1b) operating in a "burst sampling" mode, making five round trip cycles to 2000 m over 2 days (Fig. 5c) with the aim of separating internal waves from other forms of oceanic variability. Between

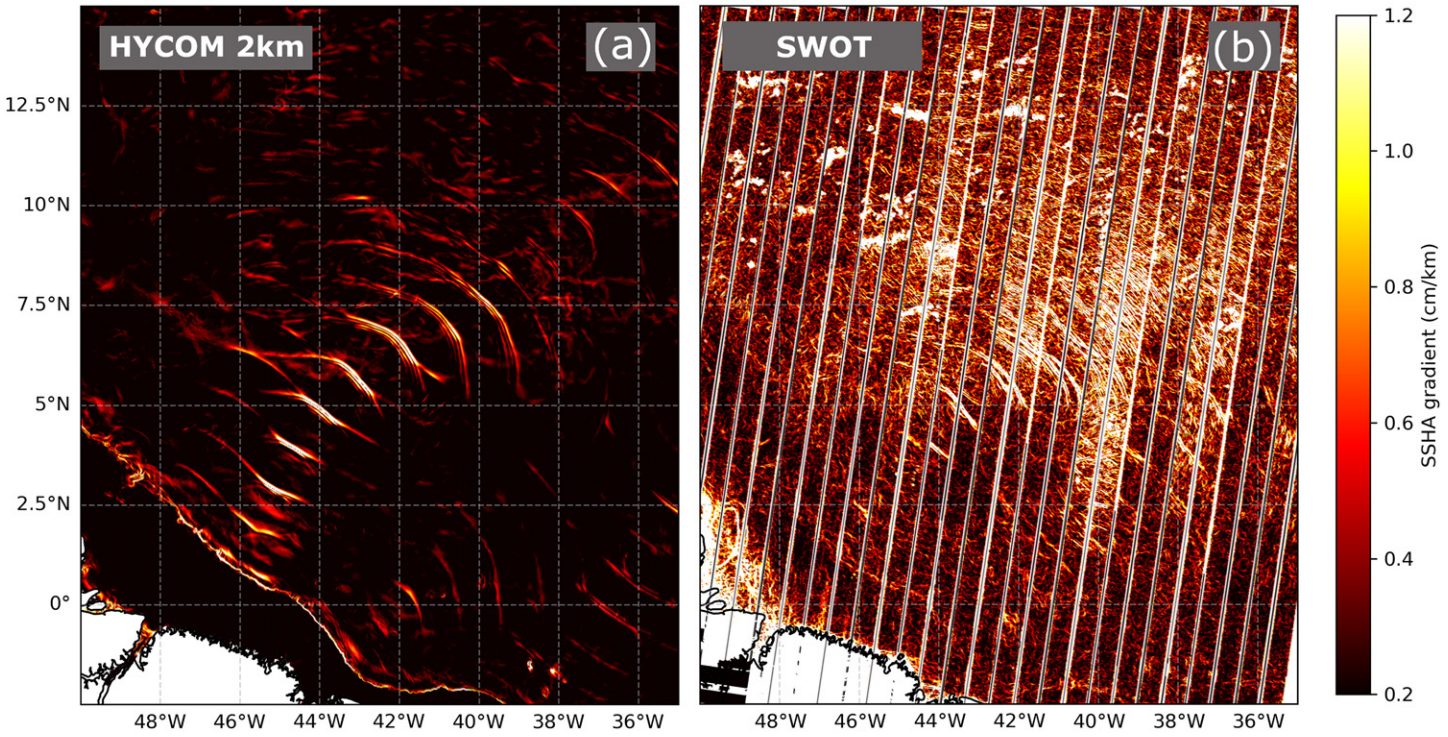

Fig. 4. Nonlinear internal tides are observed radiating from the Amazon shelf in SSH anomaly (SSHA) gradient maps based on (a) a 1/50° HYCOM simulation of the Atlantic Ocean (Xu et al. 2022) and (b) SWOT wide swath altimetry with a resolution of 2 km. SWOT data are taken during cycle 28 (2–24 Feb 2025; SWOT 2024a). The HYCOM snapshot is taken during a spring tide on 5 Jan 2017. While nonlinear internal waves are observed in both images, the SWOT data reveal much more submesoscale structure that is not resolved in the HYCOM simulation. A discussion on the dynamics of these nonlinear waves is provided in Buijsman et al. (2025).

bursts, the floats park at 1000-m depth for 10 days, again similar to the global Argo array. Overall intraburst variance gives an estimate of the broadband internal wave energy present, and harmonic analysis (Fig. 5e) enables the estimation of narrow-band signals at the dominant frequencies of tide and wind forcing (diurnal, semidiurnal, and the latitude-varying inertial frequency). The 2000-m profiling allows separation of these signals by vertical mode (Fig. 5f). In addition, the high vertical resolution of the profilers facilitates calculation of vertical wavenumber spectra for comparison with internal wave continuum models (e.g., GM76; Garrett and Munk 1975; Cairns and Williams 1976).

SQUID deployments to date have occurred on GO-SHIP large-scale hydrography lines and other cruises of opportunity, including transits and regional process studies. Floats have been launched in all of the world's oceans strong currents including the Gulf Stream and Antarctic Circumpolar Current, internal tide beams from Hawai'i, Luzon Strait, and the Mariana Ridge, and in the equatorial regions (Fig. 1b). Though previous internal wave and microstructure measurements have been made in many of these settings, the coordinated approach of a uniform measurement platform and an immediate connection to modeling output and model validation goals makes this new dataset particularly valuable.

Metrics for evaluating the success of the project will include 1) the range of internal wave statistics sampled relative to 2) the considerable uncertainties resulting from the minimal burst sampling and spectral analysis (coarse temporal resolution combined with high vertical resolution). The harmonic phase coverage and frequency separability inherent in the sampling scheme for the semidiurnal, diurnal, and inertial frequencies will result in different levels of uncertainty in different locations. However, the variance outside of each harmonic fit band will help determine the uncertainties in amplitude and phase of the resulting harmonics. 3) Direct comparisons between observed internal wave parameters, such as energy

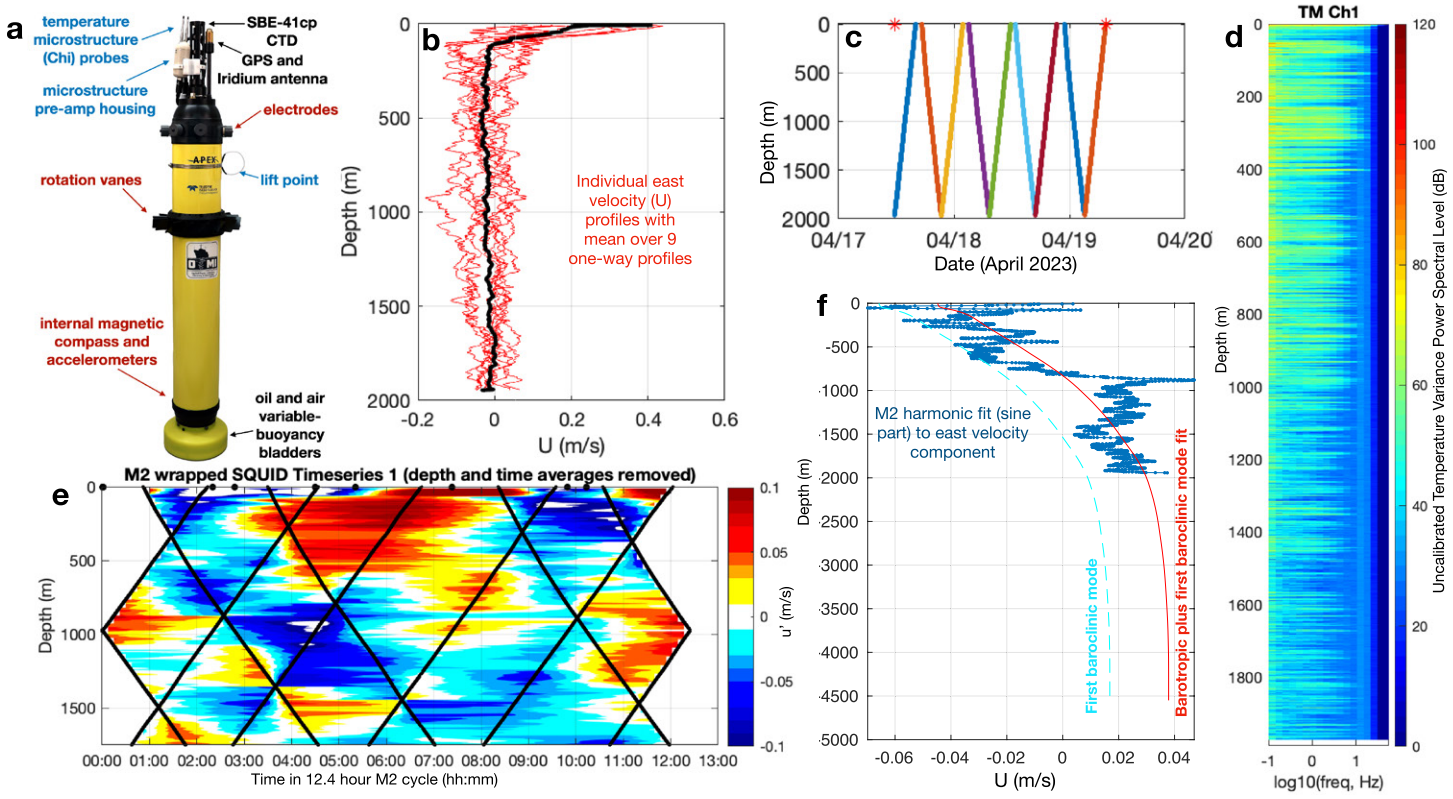

Fig. 5. (a) An EM-APEX profiling float configured as used in the NOPP GIW to collect (b) velocity profiles (east component from one 9-profile "burst") while cycling vertically to 2000 m (c). (d) Example temperature microstructure profile, showing 20-s spectra sent over Iridium. (e) A semidiurnal view of the velocity profiles in (b), with measurement times and depths (black lines) wrapped in time to a single 12.4-h M_2 tidal cycle (starting with the midpoint of the first profile in the burst). Sampling at each depth maintains relatively even (though coarse) M_2 phase coverage. (f) Illustration of vertical mode fitting to a frequency harmonic—in this case, the sine (imaginary) component of the east velocity time series at each depth.

flux of the low-mode tidal or near-inertial internal waves, with global models that resolve the wave-generation process and signal-to-noise ratio of the harmonic will be an important facet of model validation, while 4) spectral levels of high-wavenumber shear will aid the refinement of internal wave–based parameterizations for diapycnal mixing (Gregg 1989; Henyey et al. 1986; Polzin et al. 1995; Kunze et al. 2006).

4) The Distributed Sensor Network for the ocean's bottom boundary layer. Our Distributed Sensor Network is designed to investigate internal wave and subinertial flow dynamics at the ocean's bottom boundary. This effort is motivated by a lack of observations in determining the structure of the planetary boundary layer and by our limited understanding of its dynamics. For example, this has resulted in the implementation of ocean bottom boundary layer (OBBL) subgrid-scale mixing parameterizations as upside-down versions of ocean surface boundary layer (OSBL) parameterizations in ocean models (e.g., Durski et al. 2004). These mixing parameterizations ignore the phenomenology associated with sloping bathymetry that couples to critical and near-critical internal waves and topographic roughness that leads to flow blocking, splitting, separation, and internal hydraulics (Polzin and McDougall 2022). Our efforts are focused upon steep and complex topography where numerical model deficiencies can be large (Blain et al. 2025).

We achieve high spatial/temporal resolution with a Distributed Sensor Network that 1) is full-ocean-depth capable, 2) has subsecond sampling rates that enable estimates of turbulent dissipation and three-dimensional (3D) fluxes of mass, momentum, and energy in both turbulent and internal wave bands, and 3) provides realizations on multiple fortnightly and

mesoscale eddy time scales with year-long deployments. The sensors in our network are based on scalable, proven technology (Fig. 6). The unique capabilities of the network are arrived at by deploying these sensors in an array that enables us to visualize the phenomenology and quantify the physics of the ocean's bottom boundary layer that has been the source of long-standing ignorance and misunderstanding. In short, our Distributed Sensor Network aims to be a 3D antenna that resolves all, and in particular, coherent features that are especially important to determining the structure of the OBBL.

To date, individual sensor network assets have been used in a downwelling Ekman layer to document wave band motions radiating significant momentum and energy away from the OBBL. These measurements establish that the associated temperature fluxes are a key factor in restratifying the near-boundary region determining planetary boundary layer structure (Polzin et al. 2021). Similarly, sensor network assets have documented highly nonlocal temperature fluxes associated with internal Kelvin wave seiching in a canyon that appears to be the analog of a surface gravity wave shoaling on a beach (Polzin 2025). These realizations

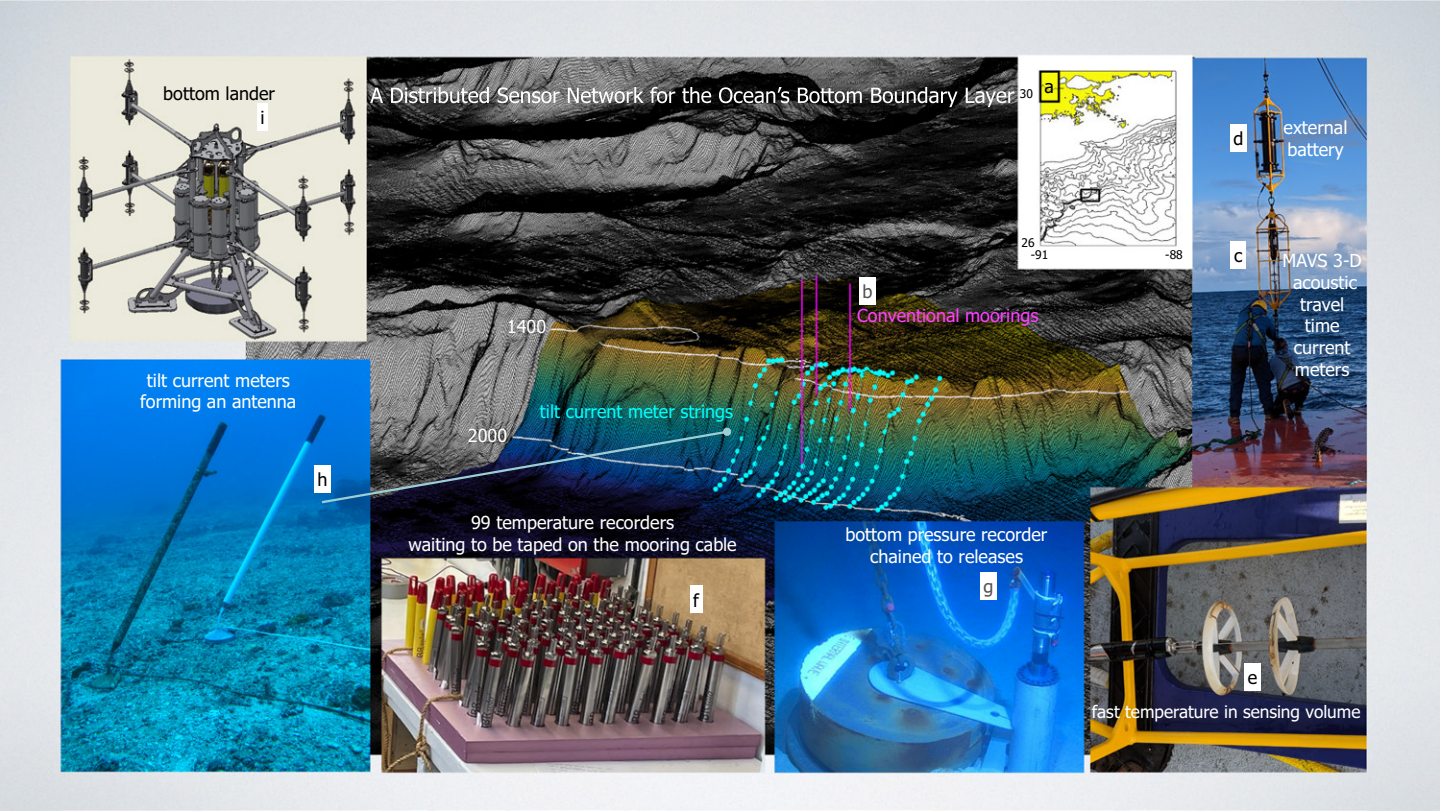

Fig. 6. (a) Distributed Sensor Network assets draped over a steep escarpment in the Gulf of Mexico. (b) The sensor network is arranged about one or more conventional taut wire moorings hosting (c) Modular Acoustic Velocity Sensor (MAVS) acoustic travel time current meters that provide estimates of 3D currents, turbulent dissipation through inertial subrange formulas, and fluxes of momentum and buoyancy at time scales of seconds to hours. (d) A single external battery pack enables 6 months of sampling at 5 Hz. (e) A serial streaming temperature recorder with a custom 10-cm-long string, whose tip is placed within the sensing volume of the acoustic current meter provides collocated temperature/velocity measurements. (f) 50 to 100 self-contained temperature recorders sampling at 0.5–1.0 Hz for a 1-yr duration are taped onto the mooring and provide high vertical resolution of internal wave and outer turbulent boundary layers. (g) Direct estimates of energy flux (pressure work) can be obtained by using the temperature recorder data to vertically integrate the hydrostatic relation and placing a bottom pressure recorder in a special frame on the anchor to provide time-varying pressure as a function of height above bottom and then combining these with the 3D currents. (h) Individual Tilt Current Meters (TCMs) are self-contained units and sample at 8 Hz with a duration of one year. In the Sensor Network, these units are deployed along lines of 6–10-km length with anchors at either end, but the nominal extent is virtually unlimited. (i) A bottom lander populated by eight MAVS current meters measuring at 0.5- and 2.5-m height above the bottom provides high vertical resolution of the turbulent OBBL, directly quantifying the frictional stress. As described, the Sensor Network is a base that can be complimented by more traditional sensors. In total, the Sensor Network assets return full resolution of turbulent and internal wave band contributions to budgets of momentum, buoyancy, vorticity, and energy.

provide us with dramatic departures from existing concepts, as discussed in Polzin and McDougall (2022), of the physical mechanisms determining the structure of the ocean's bottom boundary layer.

This Distributed Sensor Network was successfully tested recently on the northern slope of the Gulf of Mexico (Fig. 6a). A 6 × 6 km^2 grid consisting of 55 Seahorse TCMs and a vertical MAVS mooring with an additional 100 thermistors was deployed from July to November 2024. After the successful deployment and recovery cruises, analysis is underway.

b. Model simulations. In this section, we report on 1) advances in simulating tides in the global Modular Ocean Model (MOM6) simulations, 2) the skill of global HYCOM simulations in predicting the energy and phase of the internal tides, 3) improvements in data assimilation and vertical coordinates to mitigate spurious waves, and 4) the necessity of high-resolution regional- and process-level simulations to better resolve internal wave processes.

1) Global MOM6 simulations. MOM6 was developed by the Geophysical Fluid Dynamics Laboratory of the National Oceanic and Atmospheric Administration for solving the hydrostatic primitive equations in spherical polar geometry (Adcroft et al. 2019).[2] The equations of motion are discretized on a horizontal Arakawa C grid and utilize a realistic equation of state for seawater. To minimize the spurious mixing caused by numerical advection algorithms (Griffies et al. 2000; Ilicak et al. 2012), the vertical coordinate of MOM6, as in HYCOM, is Lagrangian for isentropic motions, a feature which distinguishes it from other widely used models, such as MITgcm and Regional Ocean Modeling System (ROMS). The evolution of the water column is decomposed into adiabatic and nonadiabatic dynamics, which are integrated using the arbitrary Lagrangian–Eulerian (ALE) method (White and Adcroft 2008; White et al. 2009; Griffies et al. 2020). The split-explicit time stepping method (Hallberg and Adcroft 2009) and the numerics of the pressure gradient force (Adcroft et al. 2008) are designed to be stable and accurate even in situations with steeply sloping coordinate surfaces.

[2] Ongoing development of MOM6 is being carried out by a large community consortium under an open development paradigm (https://github.com/mom-ocean/MOM6).

Activities with MOM6 in the scope of the NOPP GIW project have included a range of efforts. To build confidence in MOM6 as a tool for tide-resolving simulations, the source code was extensively reviewed, and a few minor errors in the implementation of tidal forcing were identified and corrected. To facilitate the analysis of simulation outputs, new code modules were developed to implement inline, or run-time, harmonic analysis and the computation of baroclinic sea level diagnostics (Zaron and Ray 2023). To enhance the tidal accuracy of the simulations, a frequency-dependent parameterization of topographic wave drag was implemented to represent the barotropic to baroclinic energy conversion due to unresolved internal tides and subgrid-scale wave breaking near topography (Xu and Zaron 2024). The new wave drag implementation enables the use of different latitude-dependent drag coefficient fields for the diurnal and semidiurnal frequency bands, separately from the parameterizations designed to affect the low-frequency mesoscale flows (Xu and Zaron 2025). Finally, all these features have been utilized to conduct MOM6 simulations on a global tripolar grid with nominal 1/12.5° horizontal resolution and 41 hybrid layers, similar to HYCOM, bringing MOM6 tidal simulations into approximate parity with the HYCOM-based simulations developed inside the U.S. Navy.

A series of global MOM6 simulations has been conducted to optimize the wave drag parameterization for the main semidiurnal and diurnal tidal constituents, M_2 and K_1. Comparisons of two-dimensional (2D; barotropic dynamics) and 3D (combined barotropic and baroclinic dynamics) simulations reveal the significant role of topographically trapped

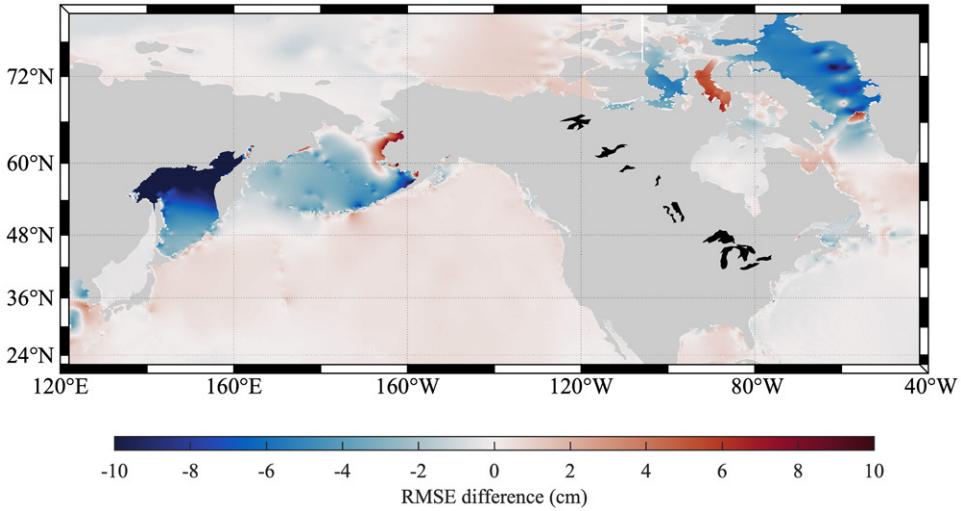

Fig. 7. Differences in the RMSE of K_1 barotropic tidal elevation between the 3D and 2D MOM6 simulations, compared with the altimeter-derived TPXO9 model. Negative values (blue) indicate more accurate representations of the tidal elevations in the 3D simulation. Improved accuracies in these regions highlight the significance of topographically trapped baroclinic waves resolved in high-resolution 3D MOM6 simulations.

subinertial waves at high latitudes, leading to more accurate results for the K_1 tide than previously obtained with global models (Figs. 7 and 8). Comparisons with satellite altimetry (TPXO9; Egbert and Erofeeva 2002) find globally averaged root-mean-square errors (RMSEs) of 2.10 and 0.85 cm, respectively, for M_2 and K_1, which were achieved simultaneously in the same simulation forced by both tidal constituents and are among the best accuracies for non-data-assimilative global simulations (Xu and Zaron 2025). The predicted baroclinic sea level also shows promising agreement with an altimeter-derived estimate [High Resolution Empirical Tides (HRET8.1); Zaron 2019], but the evaluations are more complex owing to the dependence of these waves on the large-scale stratification. The chief factors contributing to the model's accuracy are the new wave drag parameterization and the bottom topography on the tripolar grid adapted from NOAA's Global Surge and Tide Operational Forecast System (NOAA 2023).

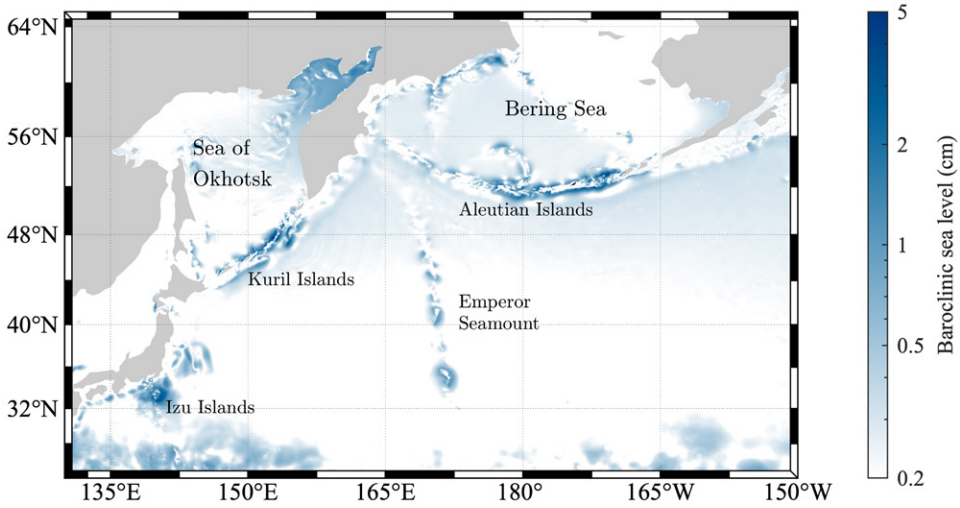

Fig. 8. Amplitude of baroclinic sea level associated with the K_1 tide in the North Pacific shows the scale of the topographically trapped subinertial waves resolved in 3D MOM6 simulations. The mixing caused by these waves is hypothesized to be a significant control on water mass properties and thus influences large-scale nontidal dynamics.

2) Global HYCOM simulations. A major goal of NOPP GIW is to assess and improve the predictability of internal tides in the Hybrid Coordinate Ocean Model, which is the dynamical core of the U.S. Navy Global Ocean Forecasting System (GOFS). To obtain accurate operational forecasts of geostrophically balanced motions, observational data are assimilated in HYCOM with the Navy Coupled Ocean Data Assimilation 3D Variational Analysis (NCODA-3DVar) System (Chassignet et al. 2009; Cummings and Smedstad 2013). Moreover, due to the inclusion of high-resolution bathymetry and optimized SAL and wave drag parameterizations, HYCOM has also become the state of the art in predicting accurate surface and internal tides when compared to other global ocean models (Arbic 2022).

Comparing HYCOM's internal tide SSH with satellite altimetry provides a direct way to assess its skill globally. In this aspect of our work, we set out to evaluate the skill of 1/25° HYCOM against three altimetric datasets: 1) nadir altimetry (JASON), 2) the Cal/Val period of the first wide-swath altimeter (SWOT), and 3) the SWOT science orbit. Previous studies (Carrère et al. 2021) have shown that non-data-assimilative HYCOM solutions are less effective at removing internal tide SSH variance from classical nadir altimeter records than empirical internal tide models because of mismatches between the predicted and observed ocean circulation. However, in Yadidya et al. (2024), we investigated the phase accuracy of a data-assimilative, tide-resolving HYCOM forecast system and found that it removes internal tide SSH variance from nadir altimetry at skill levels comparable to the state-of-the-art empirical correction model HRET8.1 (Fig. 9).

Internal tide prediction consists of both coherent (phase locked) and incoherent (nonphase locked) components. The coherent component refers to the internal tide signal that is phase

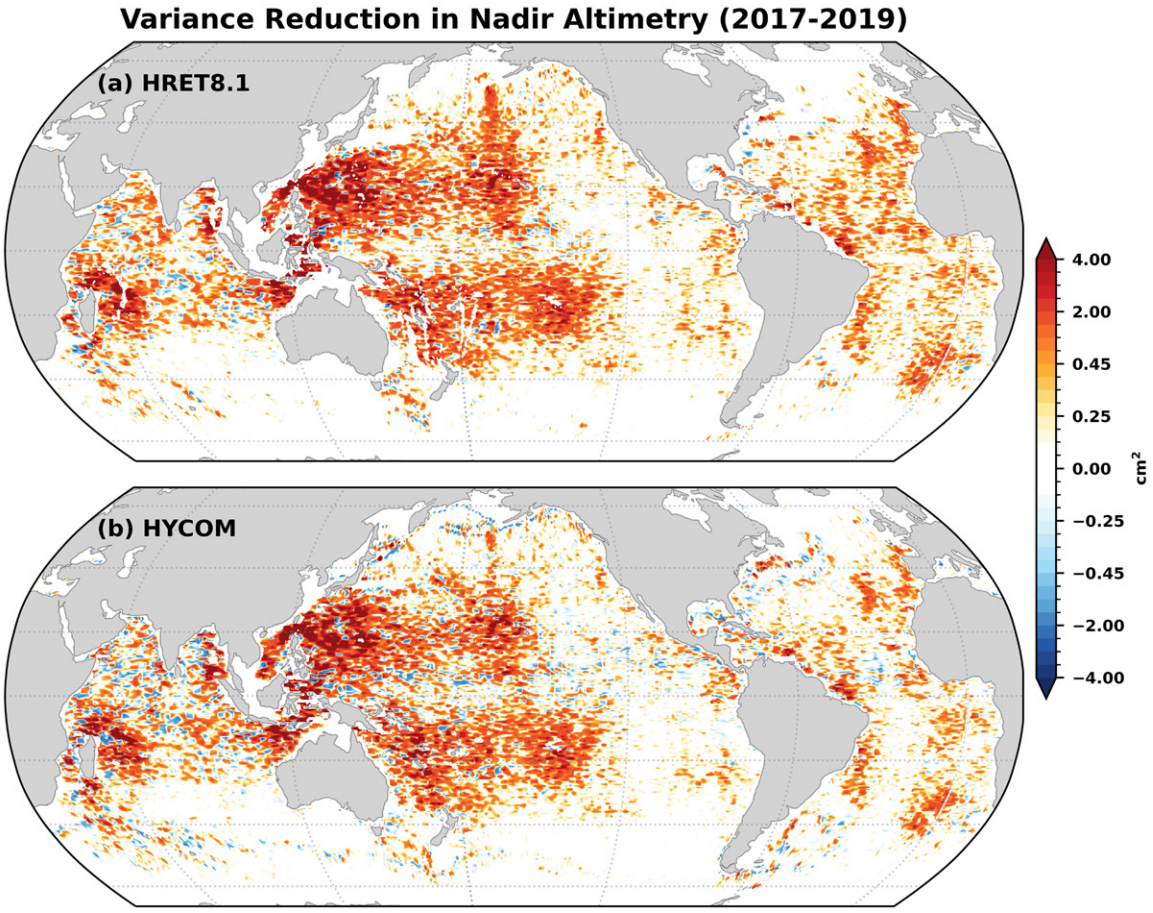

Fig. 9. Global maps of internal tide SSH variance reduction in nadir altimetry by (a) the empirical HRET8.1 model and (b) 1/25° HYCOM forecasts. The HYCOM results come from a 3-yr harmonic analysis of total SSH after applying a Gaussian spatial filter to extract the coherent internal tide signal. Adapted from Yadidya et al. (2024).

locked to the tidal forcing and thus remains consistent in amplitude and phase over multiple years—this is the portion that is well captured by harmonic analysis and by empirical models based on long-term satellite altimetry, such as HRET8.1. Incoherent (or nonphase locked) internal tide signals, in contrast, originate from tidal internal waves whose phase and amplitude vary over shorter time scales due to processes such as time-variable generation, propagation through mesoscale eddies, and other temporal modulations. These incoherent signals cannot be readily recovered by traditional harmonic analysis or by empirical models derived from nadir altimetry, but they can be predicted by a time-resolving forecast model like HYCOM, which explicitly simulates both the coherent and incoherent components and stores the model outputs at high (hourly) frequencies that allow tidal analysis over short time periods and separation of components using bandpassing. As shown in Yadidya et al. (2024), HYCOM achieves comparable or greater global variance reduction than HRET8.1, removing up to 14.7% more SSH variance when both coherent and incoherent components are included. Preliminary results from our analysis using the SWOT Cal/Val data also indicate that HYCOM removes up to 5% more coherent internal tide SSH variance than HRET22 and an additional 18.6% more incoherent variance (Yadidya et al. 2025a). These results indicate that forecast models such as HYCOM offer a novel approach for improving global internal tide mapping and altimetry corrections. Furthermore, because HYCOM explicitly represents the full water column, it serves as a valuable tool for advancing our understanding of internal tide dynamics.

3) Improvements in data assimilation and vertical coordinates. While the NCODA-3DVAR data assimilation has significantly improved HYCOM's predictive capabilities for ocean circulation over a wide range of frequencies and wavenumbers, it is not without drawbacks. The data assimilation procedure causes shocks in the positioning of mesoscale fields, and these shocks can result in spurious high-frequency internal waves in regions with strong mesoscale activity. These spurious internal waves cause an excess of energy when compared to observations and/or to simulations without data assimilation. We have been quantifying the improvements in predictions that can be obtained with either a better choice of data assimilation parameters (e.g., initialization, vertical projection, covariance, time windows, etc.) in the existing 3DVAR systems, where all ocean variables are analyzed simultaneously in three dimensions, or adoption of more sophisticated data assimilation techniques such as the four-dimensional variational data assimilation (4DVAR; Weaver 2003) and the local ensemble transform Kalman filter [LETKF; see Martin et al. (2025), for a recent review of the state of the art in data assimilation schemes for ocean forecasting].

Raja et al. (2024) demonstrate that the spurious near-inertial internal waves, generated during data updates, can be effectively mitigated by introducing smaller increments over multiple time steps during data updates, a process achieved by extending the incremental analysis update (IAU) period. The impact of different IAU periods on spurious near-inertial wave (NIW) generation was evaluated using a regional HYCOM configuration in the Gulf of Mexico, with data assimilation performed using the open-source Tendral Statistical Interpolation System (TSIS) developed by Srinivasan et al. (2022). Extending the IAU period to 24 h reduces spurious energy to 1% of NIW kinetic energy (Fig. 10), significantly improving the model's fidelity in representing internal waves.

The 4DVAR methodology provides a dynamically balanced analysis by expanding the background error covariance used by the 3DVAR method to a fourth dimension (time) via the tangent linear and adjoint of the forward model operator. The tangent linear and adjoint are used to compute derivatives of the model outputs with respect to the input parameters, which are required in the minimization process between the observations and the numerical model. Due to its time-varying vertical coordinate, the HYCOM numerical implementation

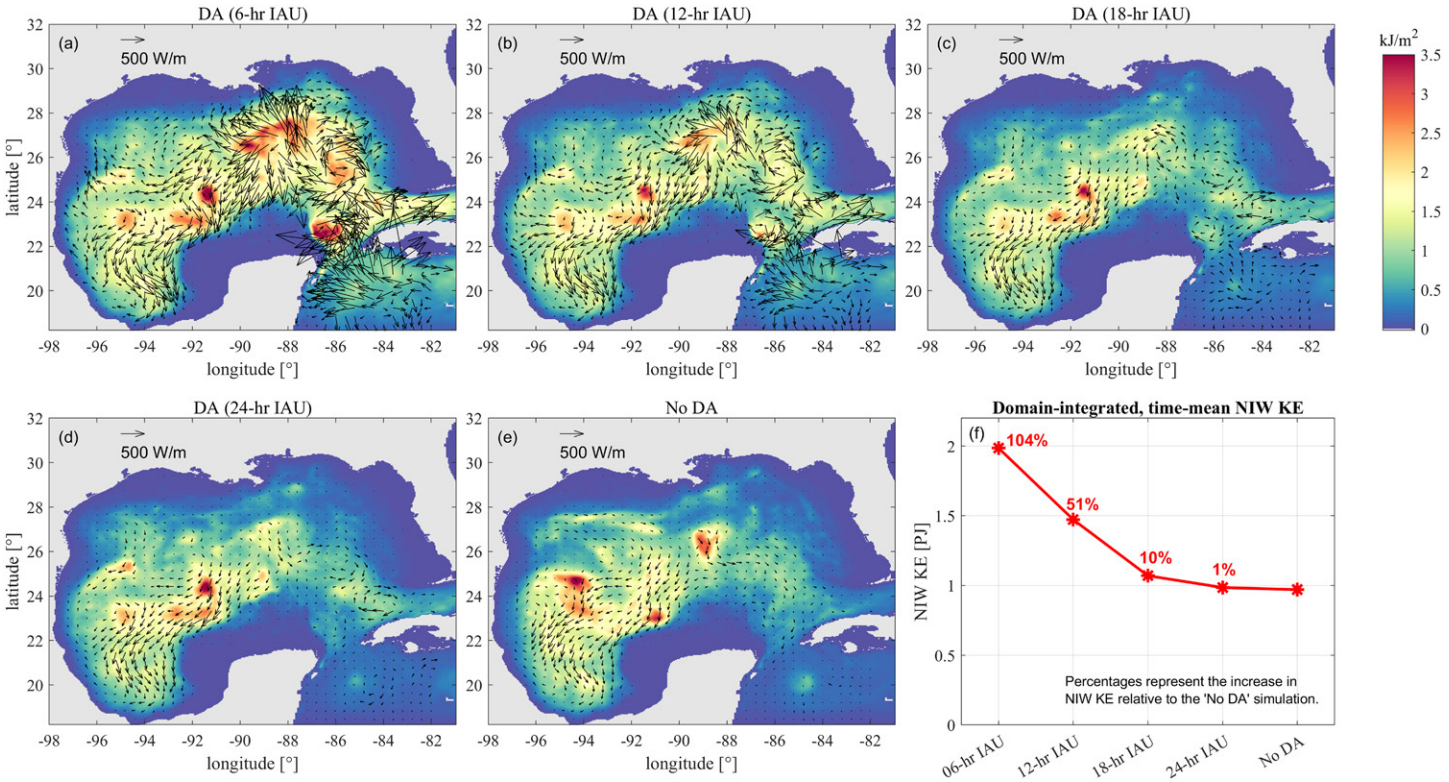

FIG. 10. The depth-integrated, time-mean NIW kinetic energy (color) and horizontal energy fluxes (vectors) in the Gulf of Mexico in simulations with (a) 6-, (b) 12-, (c) 18-, and (d) 24-h IAU, and (e) no DA. (f) Domain-integrated, time-averaged NIW kinetic energy in the Gulf of Mexico regional simulations with different IAU periods.

does not lend itself to adequate linearization and adjoint development. We have worked with the assumption that one can use the tangent linear and adjoint of another ocean model as a proxy for the operators of HYCOM, and we have developed the capability to use the NCOM-4DVAR, a 4DVAR system for the U.S. Navy Coastal Ocean Model (NCOM; Ngodock and Carrier 2014) as a proxy ocean data assimilation system for HYCOM. Over a short time period (about 120 h), an NCOM forecast is close to a HYCOM forecast if given the same initial and boundary condition states, as well as the atmospheric forcing. We have carried out a month-long numerical experiment in the Gulf of Mexico, where analysis increments are computed from the NCOM-4DVAR and added to a HYCOM forecast to make a HYCOM analysis. This HYCOM analysis is then used to initialize a new HYCOM forecast and so on. A time series comparison of analysis residuals from the existing 3DVAR and the new proxy 4DVAR for HYCOM is shown in Fig. 11, for both temperature and salinity. The residuals are computed as daily root-mean-square errors against assimilated in situ profiles. The proxy HYCOM 4DVAR produces an analysis that has significantly lower errors than the existing 3DVAR. These lower analysis errors also result in lower forecast errors (not shown). We are in the process of evaluating the amount of spurious internal waves generated by this proxy HYCOM 4DVAR approach.

Finally, another source of noise in HYCOM is thermobaric instabilities arising from the thermobaricity correction (Sun et al. 1999) used in the σ_2 potential density gradient calculation. This correction can be unstable (Hallberg 2005) if (i) temperature and salinity are far from their reference state, which is from the Atlantic, or (ii) stratification is low, i.e., isopycnal layers are thick. In the standard 41-layer global setup, layer 36 is more than 2000 m thick in the high-latitude North Pacific, and it leads to thermobaric instability in this region (Buijsman et al. 2016, 2020, 2025; Raja et al. 2022). This numerical noise mostly projects on shorter wavelength internal waves, such as high-mode semidiurnal internal waves and all modes with supertidal frequencies > 2 cycles per day (Buijsman et al. 2025). Hence, the

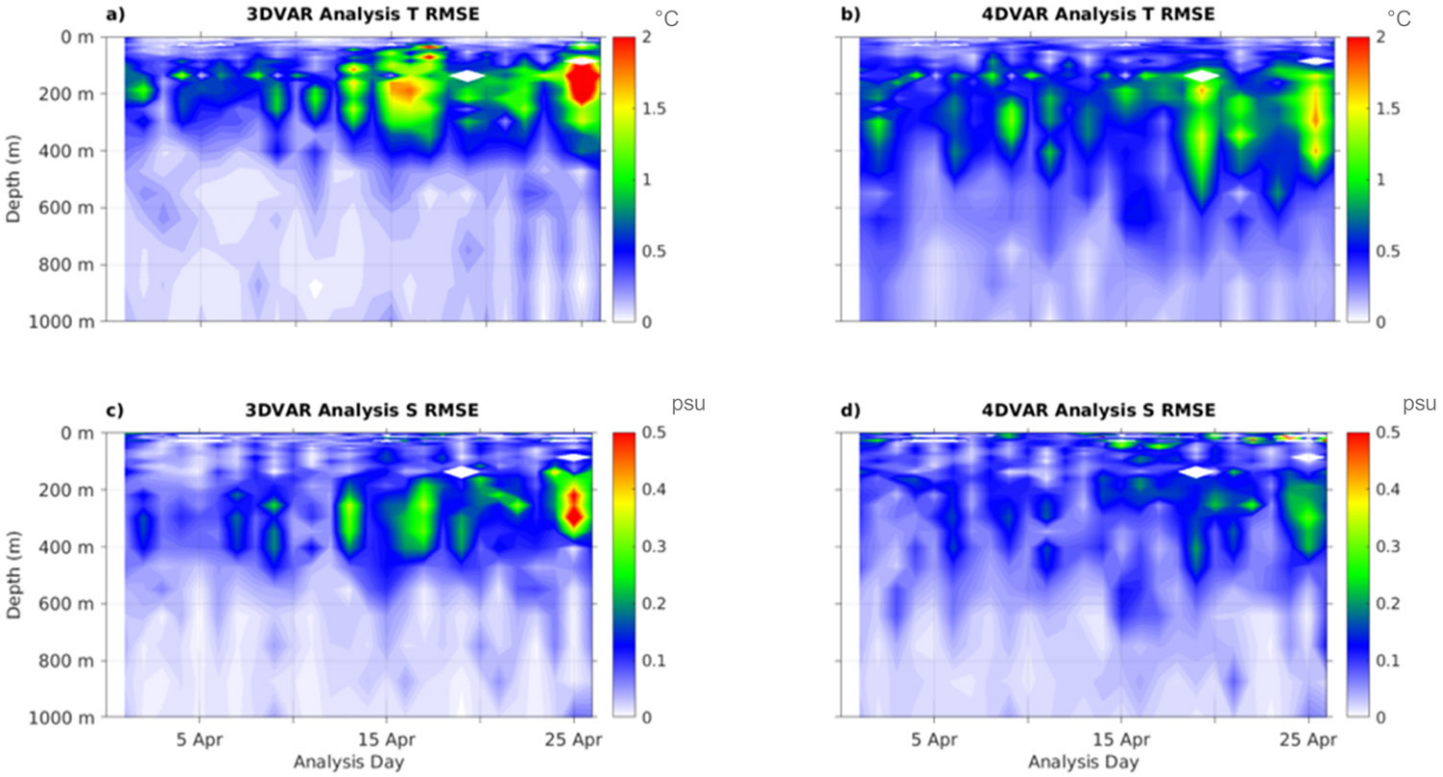

Fig. 11. A comparison of HYCOM daily analysis RMSEs from both 3DVAR and the proxy 4DVAR. Errors are for (a) 3DVAR temperature, (b) proxy 4DVAR temperature, (c) 3DVAR salinity, and (d) proxy 4DVAR salinity.

noise does not exist in the mode-1 fields in Fig. 1. We have found that the instability can be completely removed by splitting layer 36 into several layers, which can be achieved by adding new layers or by setting the maximum layer thickness to 750 m.

4) Regional and process model simulations. While the grid resolution of global simulations with tides has increased during the last decades, their resolution is not yet sufficient to accurately simulate internal-wave processes at the continental margins or to resolve the highest modes of the high-frequency internal wave spectrum in either the coastal or open ocean (Buijsman et al. 2025). Hence, it is necessary to perform coastal regional simulations, or simulations with a more developed internal wave spectrum (e.g., Thakur et al. 2022), with a higher resolution. To obtain realistic internal wave energy levels, however, these regional simulations need to be forced at the boundaries not only with surface tides and mesoscale flows but also with remote internal waves (Mazloff et al. 2020; Nelson et al. 2020).

The U.S. West Coast receives remote internal tides that were generated along the Hawaiian island ridge (Fig. 1a). Hence, the U.S. West Coast is well suited to study the impact of these remote waves on the coastal dynamics. For this reason, we have forced 1/25° ROMS (Shchepetkin and McWilliams 2005) simulations of the U.S. West Coast (red curve in Fig. 1a) with surface tides and near-inertial and tidal internal waves from a global 1/12.5° HYCOM simulation (Siyanbola et al. 2023). Compared to a ROMS simulation without remote waves (Fig. 12a), the semidiurnal internal tide energy is substantially enhanced in the simulation with remote forcing (Fig. 12b). The increase in energy levels also alters the coastal stratification through advection and vertical mixing (Siyanbola et al. 2024).

We have also employed regional and process-study model simulations to quantify which internal-wave processes are underestimated or overestimated when the horizontal grid spacing is decreased to $\mathcal{O}(1)$ km. A suite of regional simulations of the Brazilian Basin (red curve in Fig. 1a) with different grid resolutions, with and without tidal forcing, has

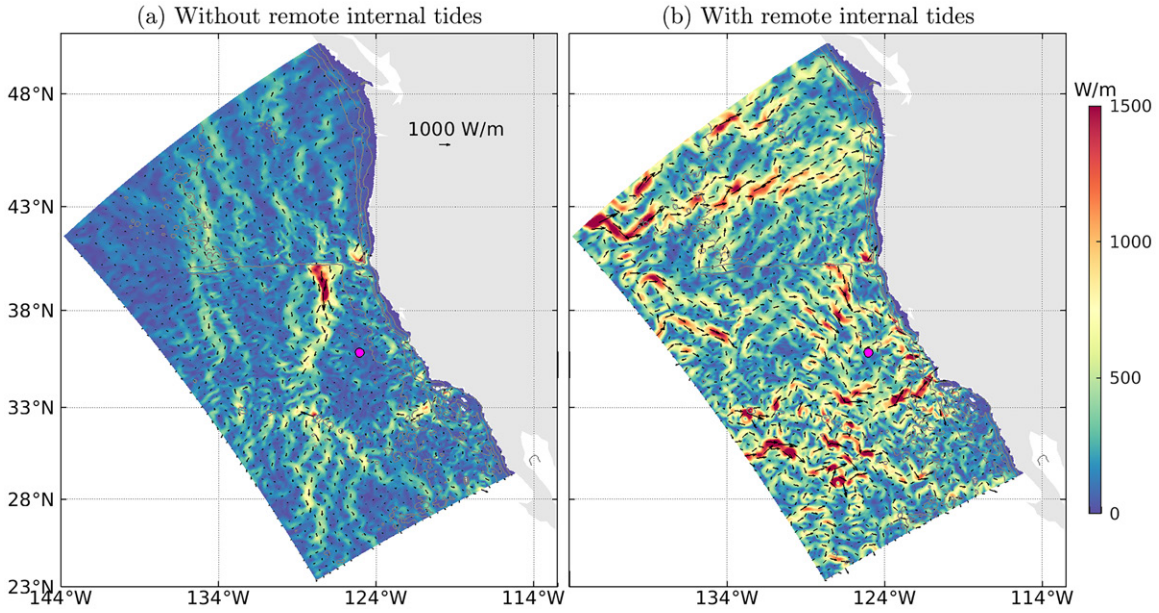

Fig. 12. Depth-integrated and time-mean (1 Jul–31 Aug 2012) semidiurnal band (1.60–2.67 cycles per day) internal wave energy fluxes for (a) a ROMS simulation without and (b) a ROMS simulation with remote internal tide forcing from a global HYCOM simulation (Siyanbola et al. 2023). The gray contours mark the 2000 and 4000 seafloor depths. The magenta-filled circle marks the IWR Array location.

revealed significant departures from the observational literature (e.g., Polzin et al. 1997) in the relative role played by submesoscale circulations and internal waves. Ocean models run at kilometer-scale resolution predict observed diapycnal diffusivity values, but the process modulating the energy and buoyancy exchanges around steep topography is vorticity generation/intensification rather than wave dynamics, as observed. This occurs because, even at such high resolution of $\mathcal{O}(1)$ km, the topography remains too smooth to block and scatter internal tides, limiting wave breaking. An example of internal wave breaking along steep topography in an idealized large-eddy simulation (LES) can be seen in Fig. 13c, where wave breaking leads to lateral intrusions with a vertical height set by the ratio of wave velocity to interior stratification, U_w/N, transporting mixed waters from the boundary into the interior (Whitley and Wenegrat 2025). These processes are absent at lower resolution, with impacts that can be framed in terms of the differences between the modeled and observed topographic height spectrum (Fig. 13a). Those differences result in a divergence between model outputs and observations in the way the energy is transferred in the system (Fig. 13b).

3. Outlook

In this paper, we have presented a snapshot of our advances in understanding and predicting the life cycle of internal waves as part of the NOPP GIW project. In what remains, we provide our perspective regarding future developments in observing, simulating, and understanding the internal wave life cycle.

A major unresolved challenge in global ocean modeling is capturing the wide range of spatial and temporal scales associated with internal wave processes. This challenge is partially addressed by ongoing advances in computing hardware, which enable the use of finer vertical and horizontal grid resolutions. For example, global MITgcm simulations have been run at 1/48° resolution (Rocha et al. 2016), and a future NOPP-funded project will include a global HYCOM simulation at 1/50° resolution. Doubling resolution takes 8× the computing power or 16× if the number of layers is also doubled. A particularly promising development is the use of graphics processing units (GPUs) which can offer more performance per dollar

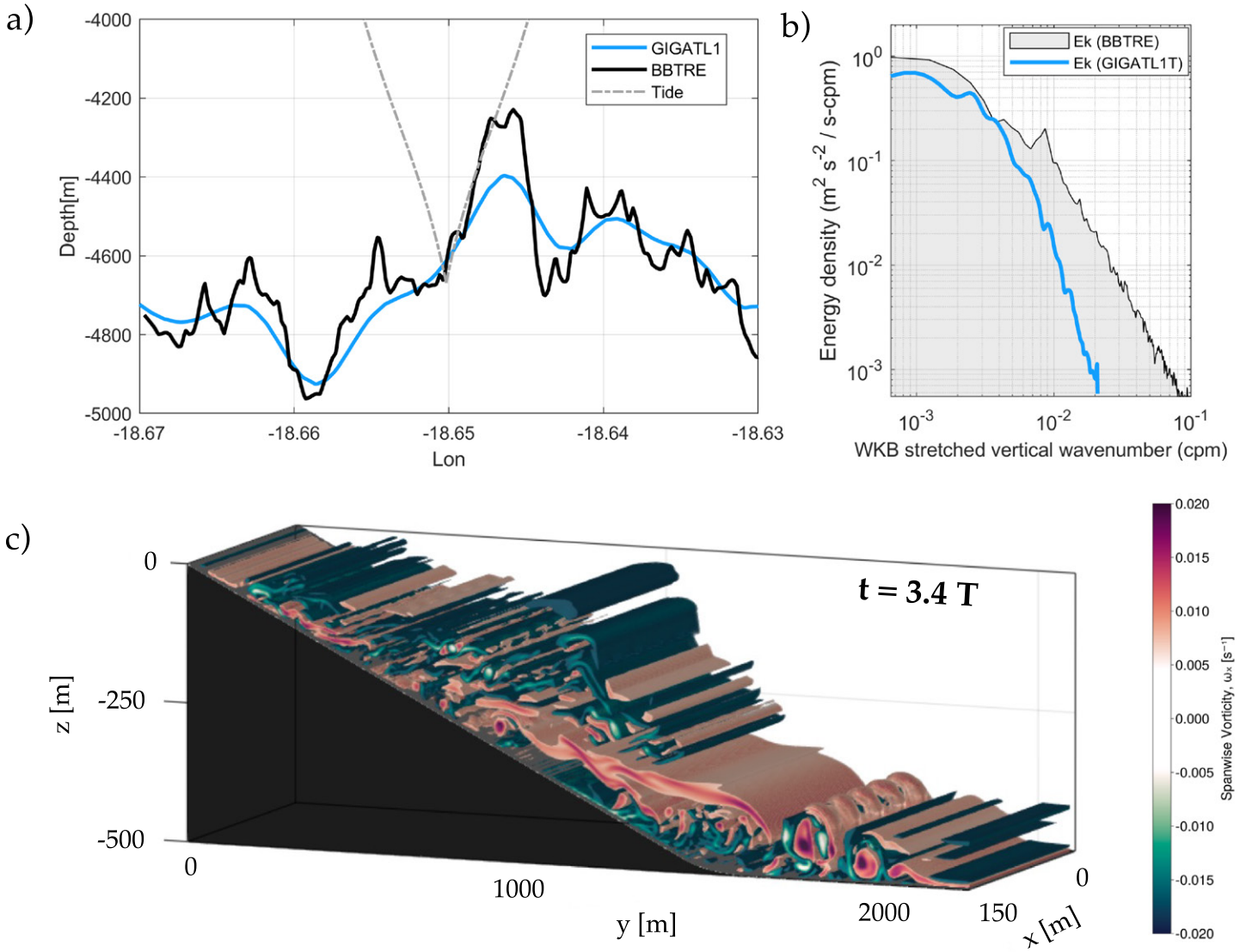

Fig. 13. (a) Topography along a transect in the Brazilian Basin as measured during the Brazilian Basin Tracer Release Experiment (BBTRE) and in a ROMS simulation at 1-km horizontal resolution (Gula et al. 2021). An example of internal wave ray trajectory at semidiurnal frequency is shown in dashed gray. (b) Stretched vertical wavenumber spectra of horizontal kinetic energy (Ek) in the ROMS simulation and BBTRE data. (c) Snapshot of spanwise vorticity from LES of a mode-1 wave breaking at supercritical topography at time $t = 3.4T$, where T is the M_2 period of the wave forcing (adapted from Whitley and Wenegrat 2025).

over traditional central processing units (CPUs). Porting existing models to GPUs may be possible but relies heavily on advanced compilers. Oceananigans.jl[3] is a new general circulation model explicitly designed to run on GPUs (Ramadhan et al. 2020; Wagner et al. 2025). This nonhydrostatic model, built on the MITgcm framework, has the potential to serve as a high-resolution global ocean modeling platform.

[3] https://clima.github.io/OceananigansDocumentation/v0.6.2/benchmarks/

Despite advances toward higher resolution in global and regional Reynolds-averaged numerical simulations (RANS), these models will not resolve internal wave breaking and the associated mixing processes in the foreseeable future. To better capture the forward energy cascade, large-eddy simulations (LESs) can be nested within high-resolution regional RANS models [e.g., the Stratified Ocean Model with Adaptive Refinement (SOMAR); Chalamalla et al. 2017]. This introduces the technical challenge of bridging intermediate grid scales where turbulence is permitted but not adequately resolved—a regime known as the "gray zone"—a well-known issue in atmospheric modeling (Chow et al. 2019). We have begun evaluating strategies for navigating the gray zone, focusing on the sensitivity of both mean-state and

turbulence statistics to closure parameterizations (Chen et al. 2025). Early results provide guidance for effective model nesting across the gray zone and suggest that true multiscale internal wave modeling is increasingly within reach.

From an operational modeling perspective, generating skillful hour-by-hour forecasts across the global ocean requires not only accurate statistical representations of the internal wave field but also correct amplitudes and phases of its dominant tidal constituents. Within the internal tide band, this depends on accurately simulating the primary forcing: the surface tide. We show that applying a frequency-dependent wave drag parameterization improves the accuracy of simulated surface tides. Another approach to enhancing surface tide predictability is barotropic nudging, in which the model tides are nudged toward altimetry-constrained solutions (e.g., Fu et al. 2021). This technique is currently being tested in 1/12.5° HYCOM simulations.

In parallel, simulating the evolving internal wave field requires assimilation of both phase and amplitude across the internal wave continuum into forecast models, which, in turn, demands continued advances in data assimilation (DA) techniques. Efforts are underway to reduce DA-related noise and to evaluate the performance of four-dimensional variational data assimilation (4DVAR) methods at global scales.

The emergence of machine learning (ML; Rumelhart et al. 1986) is increasingly impacting many areas of ocean science (Bracco et al. 2025), including the simulation and observation of internal waves. ML tools have been adopted for a range of applications: data reconstruction and downscaling (e.g., Martin et al. 2024), subgrid-scale parameterization development, enhancement or replacement of data assimilation methods, pattern recognition and feature tracking (e.g., identifying solitary waves in synthetic aperture radar images; Santos-Ferreira et al. 2025), and the integration of models and observations for data-driven prediction and forecasting (e.g., Zhang et al. 2021). While most forecasting applications to date have been limited to regional scales, such approaches may offer promising new pathways for characterizing global internal tide energy fields and their interactions (Liu et al. 2025).

Finally, improved observational techniques, strategies, and investments will also be necessary to advance toward accurate internal wave representation in ocean forecast models. Parameterized processes like ocean mixing need to be constrained on a global scale. Such efforts can build on the significant advances made in the implementation of those parameterizations in forecast models (e.g., MacKinnon et al. 2017) and similarly integrated programs such as this NOPP GIW. Recent technological advances on ocean turbulence observations are comprehensively summarized in Frajka-Williams et al. (2022). Moreover, recent innovations including instrumentation on ocean platforms such as floats (e.g., Moum et al. 2023), drifting surface platforms (e.g., Zeiden et al. 2024), underwater gliders (e.g., Carlson et al. 2025), and moorings (e.g., Miller et al. 2023; Whitwell et al. 2024) also hold great promise. New remote sensing techniques (e.g., Spence et al. 2024), distributed networks of sensors (e.g., Pelaez Quiñones et al. 2023), and distributed measurements using subsea fiber optic cables (e.g., Sinnett et al. 2020; Lucas and Pinkel 2022) are all beginning to capture the details of the 4D processes that control the forward cascade of energy from the internal wave continuum to turbulence and mixing. Comparisons of the internal wave dissipation in high-resolution global and regional models with rates inferred from turbulence observations indicate that the internal wave models discussed here are starting to show some skill in directly simulating internal wave mixing (Skitka et al. 2024a).

At the global scale, observational networks should be designed to allow for measurements that resolve the internal wave field, e.g., through a combination of novel moorings with a high vertical resolution, like the system described in section 2a, and high-resolution satellite observations such as those made by SWOT, which wide swath SSH starts to resolve highly detailed spatial structures of the global propagation of internal waves (Fig. 4). Concurrent

and collaborative improvements in model DA approaches will be necessary for these global observations to improve global forecast models in the internal wave band.

Acknowledgments. We thank the editor and the anonymous reviewers, whose contributions improved this manuscript. J. Girton and A. Moulin are supported by NSF Grant OCE-2232796. Z. Chen, V. Whitley, and J. Wenegrat are supported by NSF Grant OCE-2232441. M. Buijsman, D. Varma, B. K. Arbic, and B. Yadidya are funded by ONR Grant N0014-22-1-2576. M. Buijsman and O. Siyanbola are supported by NSF Grant OCE-1851397. E. D. Zaron and C. Xu are supported by NOAA Grant NA22OAR0110487. E. Chassignet. K. Raja, A. Wallcraft, and M. Abdulfatai are supported by ONR Grant N0014-22-1-2574. Y. Huang and A. Bracco are supported by NSF Grant OCE-2232440. J. Shriver acknowledges support from ONR Grant N00014-24-WX0-1587-01. This is NRL contribution NRL/JA/7320-25-6940 and has been approved for public release. A. F. Waterhouse, A. J. Lucas, U. Send, M. Lankhorst, G. Meiners, C. Griffin, M. Andres, and T. Farrar are funded by ONR Grant N00014-22-1-2575. J. Wang is supported by NASA Grant 80NSSC25K7870.

Data availability statement. The first 1.5 years of SQUID profiling float data are available at https://www.ncei.noaa.gov/archive/accession/0305618. The MOM6 source code is available at https://github.com/NOAA-GFDL/MOM6. The input data files for recreating the MOM6 simulations used here are associated with https://doi.org/10.5281/zenodo.16905128. Diagnosed energy terms from the ROMS simulations of the U.S. West Coast are available at https://doi.org/10.5281/zenodo.7194957. The semidiurnal and near-inertial fields of modal energy terms for the 1/25° global HYCOM simulation are available at https://doi.org/10.5281/zenodo.6643378 and https://doi.org/10.5281/zenodo.5765438, respectively. Global maps of internal tide SSH variance reduction in nadir altimetry can be reproduced using data from Yadidya (2023), while the internal tide SSH corrections for the SWOT Cal/Val period, derived from the HYCOM forecast system, are available at Yadidya et al. (2025b). The data shown in Fig. 3 from the IWR array mooring and CPIESs are publicly available from NASA PO.DAAC (Physical Oceanography Distributed Active Archive Center) at https://doi.org/10.5067/SWTPO-MOOR2 and https://doi.org/10.5281/zenodo.17211193, respectively. The SWOT data used in Fig. 4 can be accessed from PO.DAAC following https://podaac.jpl.nasa.gov/dataset/SWOT_L2_LR_SSH_2.0.

References

Adcroft, A., R. Hallberg, and M. Harrison, 2008: A finite volume discretization of the pressure gradient force using analytic integration. *Ocean Modell.*, **22**, 106–113, https://doi.org/10.1016/j.ocemod.2008.02.001.

——, and Coauthors, 2019: The GFDL global ocean and sea ice model OM4.0: Model description and simulation features. *J. Adv. Model. Earth Syst.*, **11**, 3167–3211, https://doi.org/10.1029/2019MS001726.

Alford, M. H., 2001: Internal swell generation: The spatial distribution of energy flux from the wind to mixed layer near-inertial motions. *J. Phys. Oceanogr.*, **31**, 2359–2368, https://doi.org/10.1175/1520-0485(2001)031<2359:ISGTSD>2.0.CO;2.

Andres, M., 2025: National Ocean Partnership Program Global Internal Wave Study: California Internal Wave Resolving Array—L3 Hourly CPIES Data version 1. Zenodo, accessed 26 September 2025, https://doi.org/10.5281/zenodo.17211193.

Arbic, B. K., 2022: Incorporating tides and internal gravity waves within global ocean general circulation models: A review. *Prog. Oceanogr.*, **206**, 102824, https://doi.org/10.1016/j.pocean.2022.102824.

——, S. T. Garner, R. W. Hallberg, and H. L. Simmons, 2004: The accuracy of surface elevations in forward global barotropic and baroclinic tide models. *Deep-Sea Res. II*, **51**, 3069–3101, https://doi.org/10.1016/j.dsr2.2004.09.014.

——, A. J. Wallcraft, and E. J. Metzger, 2010: Concurrent simulation of the eddying general circulation and tides in a global ocean model. *Ocean Modell.*, **32**, 175–187, https://doi.org/10.1016/j.ocemod.2010.01.007.

——, and Coauthors, 2018: A primer on global internal tide and internal gravity wave continuum modeling in HYCOM and MITgcm. *New Frontiers in Operational Oceanography*, E. Chassignet et al., Eds., GODAE OceanView, 307–392, https://doi.org/10.17125/gov2018.ch13.

Archer, M., J. Wang, P. Klein, G. Dibarboure, and L.-L. Fu, 2025: Wide-swath satellite altimetry unveils global submesoscale ocean dynamics. *Nature*, **640**, 691–696, https://doi.org/10.1038/s41586-025-08722-8.

Blain, C. A., Z. Yu, and T. R. Campbell, 2025: Sea bottom warfare: Predicting deep ocean currents in the South China Sea. NRL Memo. Tech. Rep. IR-7232-25-2-U, 44 pp.

Bleck, R., 2002: An oceanic general circulation model framed in hybrid isopycnic-Cartesian coordinates. *Ocean Modell.*, **4**, 55–88, https://doi.org/10.1016/S1463-5003(01)00012-9.

Boegman, L., and M. Stastna, 2019: Sediment resuspension and transport by internal solitary waves. *Annu. Rev. Fluid Mech.*, **51**, 129–154, https://doi.org/10.1146/annurev-fluid-122316-045049.

Bracco, A., J. Brajard, H. A. Dijkstra, P. Hassanzadeh, C. Lessig, and C. Monteleoni, 2025: Machine learning for the physics of climate. *Nat. Rev. Phys.*, **7**, 6–20, https://doi.org/10.1038/s42254-024-00776-3.

Briscoe, M. G., 1975: Internal waves in the ocean. *Rev. Geophys.*, **13**, 591–598, https://doi.org/10.1029/RG013i003p00591.

Buijsman, M. C., B. K. Arbic, J. Green, R. W. Helber, J. G. Richman, J. F. Shriver, P. Timko, and A. Wallcraft, 2015: Optimizing internal wave drag in a forward barotropic model with semidiurnal tides. *Ocean Modell.*, **85**, 42–55, https://doi.org/10.1016/j.ocemod.2014.11.003.

——, and Coauthors, 2016: Impact of parameterized internal wave drag on the semidiurnal energy balance in a global ocean circulation model. *J. Phys. Oceanogr.*, **46**, 1399–1419, https://doi.org/10.1175/JPO-D-15-0074.1.

——, B. K. Arbic, S. M. Kelly, and A. F. Waterhouse, 2019: Internal gravity waves. *Encyclopedia of Ocean Sciences*, 3rd ed. Academic Press, 622–632, https://doi.org/10.1016/B978-0-12-409548-9.04160-9.

——, and Coauthors, 2020: On the interplay between horizontal resolution and wave drag and their effect on tidal baroclinic mode waves in realistic global ocean simulations. *Ocean Modell.*, **152**, 101656, https://doi.org/10.1016/j.ocemod.2020.101656.

——, and Coauthors, 2025: Energetics of (super)tidal baroclinic modes in a realistically forced global ocean simulation. *J. Geophys. Res. Oceans*, **130**, e2025JC022460, https://doi.org/10.1029/2025JC022460.

Cairns, J. L., and G. O. Williams, 1976: Internal wave observations from a midwater float, 2. *J. Geophys. Res.*, **81**, 1943–1950, https://doi.org/10.1029/JC081i012p01943.

Carlson, D., L. Merkelbach, and J. Carpenter, 2025: Measuring ocean turbulence under extreme storm conditions using helicopter-deployed ocean gliders. *EGU General Assembly*, Vienna, Austria, European Geophysical Union, EGU25-16184, https://doi.org/10.5194/egusphere-egu25-16184.

Carrère, L., and Coauthors, 2021: Accuracy assessment of global internal-tide models using satellite altimetry. *Ocean Sci.*, **17**, 147–180, https://doi.org/10.5194/os-17-147-2021.

Chalamalla, V. K., E. Santilli, A. Scotti, M. Jalali, and S. Sarkar, 2017: SOMAR-LES: A framework for multi-scale modeling of turbulent stratified oceanic flows. *Ocean Modell.*, **120**, 101–119, https://doi.org/10.1016/j.ocemod.2017.11.003.

Chassignet, E., and Coauthors, 2009: US GODAE: Global ocean prediction with the HYbrid Coordinate Ocean Model (HYCOM). *Oceanography*, **22** (2), 64–75, https://doi.org/10.5670/oceanog.2009.39.

Chen, S.-T., D.-J. Li, H. Tian, J.-Y. Hou, D.-Y. Ning, and Y.-J. Gong, 2022: Experimental study of the effect of internal waves on the rotational hydrodynamics of underwater vehicle. *Int. J. Nav. Archit. Ocean Eng.*, **14**, 100465, https://doi.org/10.1016/j.ijnaoe.2022.100465.

Chen, Z., J. Wenegrat, T. Chor, and P. Marchesiello, 2025: Evaluating turbulence parameterizations at gray zone resolutions for the ocean surface boundary layer. *J. Adv. Model. Earth Syst.*, **17**, e2025MS005104, https://doi.org/10.1029/2025MS005104.

Chow, F., C. Schar, N. Ban, K. Lundquist, L. Schlemmer, and X. Shi, 2019: Crossing multiple gray zones in the transition from mesoscale to microscale simulation over complex terrain. *Atmosphere*, **10**, 274, https://doi.org/10.3390/atmos10050274.

Colosi, J. A., 2016: *Sound Propagation through the Stochastic Ocean.* Cambridge University Press, 420 pp.

Cummings, J. A., and O. M. Smedstad, 2013: Variational data assimilation for the global ocean. *Data Assimilation for Atmospheric, Oceanic and Hydrologic Applications*, Vol. II, S. K. Park and L. Xu, Eds., Springer-Verlag, 303–343.

Durski, S. M., S. M. Glenn, and D. B. Haidvogel, 2004: Vertical mixing schemes in the coastal ocean: Comparison of the level 2.5 Mellor-Yamada scheme with an enhanced version of the K profile parameterization. *J. Geophys. Res.*, **109**, C01015, https://doi.org/10.1029/2002JC001702.

Dushaw, B. D., B. M. Howe, B. D. Cornuelle, P. F. Worcester, and D. S. Luther, 1995: Barotropic and baroclinic tides in the central North Pacific Ocean determined from long-range reciprocal acoustic transmissions. *J. Phys. Oceanogr.*, **25**, 631–647, https://doi.org/10.1175/1520-0485(1995)025<0631:BABTIT>2.0.CO;2.

Egbert, G. D., and R. D. Ray, 2000: Significant dissipation of tidal energy in the deep ocean inferred from satellite altimeter data. *Nature*, **405**, 775–778, https://doi.org/10.1038/35015531.

——, and S. Y. Erofeeva, 2002: Efficient inverse modeling of barotropic ocean tides. *J. Atmos. Oceanic Technol.*, **19**, 183–204, https://doi.org/10.1175/1520-0426(2002)019<0183:EIMOBO>2.0.CO;2.

Flexas, M. M., A. F. Thompson, H. S. Torres, P. Klein, J. T. Farrar, H. Zhang, and D. Menemenlis, 2019: Global estimates of the energy transfer from the wind to the ocean, with emphasis on near-inertial oscillations. *J. Geophys. Res. Oceans*, **124**, 5723–5746, https://doi.org/10.1029/2018JC014453.

Frajka-Williams, E., J. A. Brearley, J. D. Nash, and C. B. Whalen, 2022: New technological frontiers in ocean mixing. *Ocean Mixing*, M. Meredith and A. Naveira Garabato, Eds., Elsevier, 345–361, https://doi.org/10.1016/B978-0-12-821512-8.00021-9.

Fu, H., X. Wu, W. Li, L. Zhang, K. Liu, and B. Dan, 2021: Improving the accuracy of barotropic and internal tides embedded in a high-resolution global ocean circulation model of MITgcm. *Ocean Modell.*, **162**, 101 809, https://doi.org/10.1016/j.ocemod.2021.101809.

Furuichi, N., T. Hibiya, and Y. Niwa, 2008: Model-predicted distribution of wind-induced internal wave energy in the world's oceans. *J. Geophys. Res.*, **113**, C09034, https://doi.org/10.1029/2008JC004768.

Garrett, C., and W. Munk, 1975: Space-time scales of internal waves: A progress report. *J. Geophys. Res.*, **80**, 291–297, https://doi.org/10.1029/JC080i003p00291.

——, and ——, 1979: Internal waves in the ocean. *Annu. Rev. Fluid Mech.*, **11**, 339–369, https://doi.org/10.1146/annurev.fl.11.010179.002011.

Gill, A. E., 1982: *Atmosphere-Ocean Dynamics.* International Geophysics Series, Vol. 30, Academic Press, 662 pp.

Gregg, M. C., 1989: Scaling turbulent dissipation in the thermocline. *J. Geophys. Res.*, **94**, 9686–9698, https://doi.org/10.1029/JC094iC07p09686.

Griffies, S. M., R. C. Pacanowski, and R. W. Hallberg, 2000: Spurious diapycnal mixing associated with advection in a *z*-coordinate ocean model. *Mon. Wea. Rev.*, **128**, 538–564, https://doi.org/10.1175/1520-0493(2000)128<0538:SDMAWA>2.0.CO;2.

——, A. Adcroft, and R. W. Hallberg, 2020: A primer on the vertical Lagrangian-remap method in ocean models based on finite volume generalized vertical coordinates. *J. Adv. Model. Earth Syst.*, **12**, e2019MS001954, https://doi.org/10.1029/2019MS001954.

Gula, J., S. Theetten, G. Cambon, and G. Roullet, 2021: Description of the GIGATL simulations. Version v1.1. Zenodo, https://doi.org/10.5281/ZENODO.4948523.

Hallberg, R., 2005: A thermobaric instability of Lagrangian vertical coordinate ocean models. *Ocean Modell.*, **8**, 279–300, https://doi.org/10.1016/j.ocemod.2004.01.001.

——, and A. J. Adcroft, 2009: Reconciling estimates of the free surface height in Lagrangian vertical coordinate ocean models with mode-split time stepping. *Ocean Modell.*, **29**, 15–26, https://doi.org/10.1016/j.ocemod.2009.02.008.

Headrick, R. H., and Coauthors, 2000: Acoustic normal mode fluctuation statistics in the 1995 SWARM internal wave scattering experiment. *J. Acoust. Soc. Amer.*, **107**, 201–220, https://doi.org/10.1121/1.428563.

Henyey, F. S., J. Wright, and S. M. Flatté, 1986: Energy and action flow through the internal wave field: An eikonal approach. *J. Geophys. Res.*, **91**, 8487–8495, https://doi.org/10.1029/JC091iC07p08487.

Hiron, L., and Coauthors, 2025: The influence of vertical resolution on internal tide energetics and subsequent effects on underwater acoustic propagation. *J. Adv. Model. Earth Syst.*, **17**, e2024MS004389, https://doi.org/10.1029/2024MS004389.

Ilicak, M., A. J. Adcroft, S. M. Griffies, and R. W. Hallberg, 2012: Spurious dianeutral mixing and the role of momentum closure. *Ocean Modell.*, **45–46**, 37–58, https://doi.org/10.1016/j.ocemod.2011.10.003.

Jochum, M., B. P. Briegleb, G. Danabasoglu, W. G. Large, N. J. Norton, S. R. Jayne, M. H. Alford, and F. O. Bryan, 2013: The impact of oceanic near-inertial waves on climate. *J. Climate*, **26**, 2833–2844, https://doi.org/10.1175/JCLI-D-12-00181.1.

Kelly, S. M., N. L. Jones, J. D. Nash, and A. F. Waterhouse, 2013: The geography of semidiurnal mode-1 internal-tide energy loss. *Geophys. Res. Lett.*, **40**, 4689–4693, https://doi.org/10.1002/grl.50872.

Kumar, N., and Coauthors, 2021: The inner-shelf dynamics experiment. *Bull. Amer. Meteor. Soc.*, **102**, E1033–E1063, https://doi.org/10.1175/BAMS-D-19-0281.1.

Kunze, E., E. Firing, J. Hummon, T. K. Chereskin, and A. M. Thurnherr, 2006: Global abyssal mixing inferred from lowered ADCP shear and CTD strain profiles. *J. Phys. Oceanogr.*, **36**, 1553–1576, https://doi.org/10.1175/JPO2926.1.

Lien, R.-C., T. B. Sanford, J. A. Carlson, and J. H. Dunlap, 2016: Autonomous microstructure EM-APEX floats. *Methods Oceanogr.*, **17**, 282–295, https://doi.org/10.1016/j.mio.2016.09.003.

Little, A. D., 1966: Internal waves: Their influence upon naval operations. Dept. of the Navy Bureau of Ships Tech. Rep. Sf-101-03-21, 32 pp., https://apps.dtic.mil/sti/tr/pdf/AD0632010.pdf.

Liu, S., Z. Xu, J. You, P. Zhang, X. Li, and Z. Cai, 2025: Deep learning forecast of semidiurnal internal tides from the Mariana Arc. *J. Geophys. Res. Mach. Learn. Comput.*, **2**, e2024JH000363, https://doi.org/10.1029/2024JH000363.

Lucas, A. J., and R. Pinkel, 2022: Observations of coherent transverse wakes in shoaling nonlinear internal waves. *J. Phys. Oceanogr.*, **52**, 1277–1293, https://doi.org/10.1175/JPO-D-21-0059.1.

——, P. Franks, and C. Dupont, 2011: Horizontal internal-tide fluxes support elevated phytoplankton productivity over the inner continental shelf. *Limnol. Oceanogr.*, **1**, 56–74, https://doi.org/10.1215/21573698-1258185.

Luecke, C. A., and Coauthors, 2017: The global mesoscale eddy available potential energy field in models and observations. *J. Geophys. Res. Oceans*, **122**, 9126–9143, https://doi.org/10.1002/2017JC013136.

Lynch, J. F., Y.-T. Lin, T. F. Duda, and A. E. Newhall, 2010: Acoustic ducting, reflection, refraction, and dispersion by curved nonlinear internal waves in shallow water. *IEEE J. Oceanic Eng.*, **35**, 12–27, https://doi.org/10.1109/JOE.2009.2038512.

MacKinnon, J. A., and Coauthors, 2017: Climate process team on internal wave-driven ocean mixing. *Bull. Amer. Meteor. Soc.*, **98**, 2429–2454, https://doi.org/10.1175/BAMS-D-16-0030.1.

Martin, M. J., I. Hoteit, L. Bertino, and A. M. Moore, 2025: Data assimilation schemes for ocean forecasting: State of the art. *Ocean Prediction: Present Status and State of the Art (OPSR)*, State Planet, 5-opsr, Copernicus Publications, 9 pp., https://doi.org/10.5194/sp-5-opsr-9-2025.

Martin, S. A., G. E. Manucharyan, and P. Klein, 2024: Deep learning improves global satellite observations of ocean eddy dynamics. *Geophys. Res. Lett.*, **51**, e2024GL110059, https://doi.org/10.1029/2024GL110059.

Mazloff, M. R., B. Cornuelle, S. T. Gille, and J. Wang, 2020: The importance of remote forcing for regional modeling of internal waves. *J. Geophys. Res. Oceans*, **125**, e2019JC015623, https://doi.org/10.1029/2019JC015623.

Melet, A., R. Hallberg, S. Legg, and K. Polzin, 2013a: Sensitivity of the ocean state to the vertical distribution of internal-tide-driven mixing. *J. Phys. Oceanogr.*, **43**, 602–615, https://doi.org/10.1175/JPO-D-12-055.1.

——, M. Nikurashin, C. Muller, S. Falahat, J. Nycander, P. G. Timko, B. K. Arbic, and J. A. Goff, 2013b: Internal tide generation by abyssal hills using analytical theory. *J. Geophys. Res. Oceans*, **118**, 6303–6318, https://doi.org/10.1002/2013JC009212.

——, R. Hallberg, S. Legg, and M. Nikurashin, 2014: Sensitivity of the ocean state to lee wave–driven mixing. *J. Phys. Oceanogr.*, **44**, 900–921, https://doi.org/10.1175/JPO-D-13-072.1.

——, ——, A. Adcroft, M. Nikurashin, and S. Legg, 2015: Energy flux into internal lee waves: Sensitivity to future climate changes using linear theory and a climate model. *J. Climate*, **28**, 2365–2384, https://doi.org/10.1175/JCLI-D-14-00432.1.

——, S. Legg, and R. Hallberg, 2016: Climatic impacts of parameterized local and remote tidal mixing. *J. Climate*, **29**, 3473–3500, https://doi.org/10.1175/JCLI-D-15-0153.1.

Miller, U. K., C. J. Zappa, S. F. Zippel, J. T. Farrar, and R. A. Weller, 2023: Scaling of moored surface ocean turbulence measurements in the Southeast Pacific Ocean. *J. Geophys. Res. Oceans*, **128**, e2022JC018901, https://doi.org/10.1029/2022JC018901.

Moum, J. N., and Coauthors, 2023: Flippin' χSOLO, an upper-ocean autonomous turbulence-profiling float. *J. Atmos. Oceanic Technol.*, **40**, 629–644, https://doi.org/10.1175/JTECH-D-22-0067.1.

Müller, P., G. Holloway, F. Henyey, and N. Pomphrey, 1986: Nonlinear interactions among internal gravity waves. *Rev. Geophys.*, **24**, 493–536, https://doi.org/10.1029/RG024i003p00493.

Müller, M., J. Cherniawsky, M. Foreman, and J. von Storch, 2012: Global M_2 internal tide and its seasonal variability from high resolution ocean circulation and tide modeling. *Geophys. Res. Lett.*, **39**, L19607, https://doi.org/10.1029/2012GL053320.

——, B. Arbic, J. Richman, J. Shriver, E. Kunze, R. B. Scott, A. Wallcraft, and L. Zamudio, 2015: Toward an internal gravity wave spectrum in global ocean models. *Geophys. Res. Lett.*, **42**, 3474–3481, https://doi.org/10.1002/2015GL063365.

Munk, W., 1981: Internal waves and small-scale processes. *Evolution of Physical Oceanography*, B. A. Warren and C. Wunsch, Eds., MIT Press, 264–281.

——, and C. Wunsch, 1998: Abyssal recipes II: Energetics of tidal and wind mixing. *Deep-Sea Res. I*, **45**, 1977–2010, https://doi.org/10.1016/S0967-0637(98)00070-3.

Nansen, F., 1897: *Farthest North: The Epic Adventure of a Visionary Explorer*. Skyhorse Publishing, 528 pp.

Nelson, A. D., B. K. Arbic, D. Menemenlis, W. R. Peltier, M. H. Alford, N. Grisouard, and J. M. Klymak, 2020: Improved internal wave spectral continuum in a regional ocean model. *J. Geophys. Res. Oceans*, **125**, e2019JC015974, https://doi.org/10.1029/2019JC015974.

Neuman, S., 2021: What is an 'internal wave'? It might explain the loss of an Indonesian submarine. National Public Radio, https://www.npr.org/2021/04/30/992496772/what-is-an-internal-wave-it-might-explain-the-loss-of-an-indonesian-submarine.

Ngodock, H. E., and M. J. Carrier, 2014: A 4DVAR system for the navy coastal ocean model. Part II: Strong and weak constraint assimilation experiments with real observations in Monterey Bay. *Mon. Wea. Rev.*, **142**, 2108–2117, https://doi.org/10.1175/MWR-D-13-00220.1.

——, I. Souopgui, A. J. Wallcraft, J. G. Richman, J. F. Shriver, and B. K. Arbic, 2016: On improving the accuracy of the M_2 barotropic tides embedded in a high-resolution global ocean circulation model. *Ocean Modell.*, **97**, 16–26, https://doi.org/10.1016/j.ocemod.2015.10.011.

Niwa, Y., and T. Hibiya, 2001: Numerical study of the spatial distribution of the M_2 internal tide in the Pacific Ocean. *J. Geophys. Res.*, **106**, 22 441–22 449, https://doi.org/10.1029/2000JC000770.

NOAA, 2023: NOAA Global surge and tide operational forecast system 2-D (STOFS-2D-Global). Accessed 3 February 2023, https://doi.org/10.25923/ng4h-4b85.

Pelaez Quiñones, J. D., and Coauthors, 2023: High resolution seafloor thermometry for internal wave and upwelling monitoring using distributed acoustic sensing. *Sci. Rep.*, **13**, 17459, https://doi.org/10.1038/s41598-023-44635-0.

Pinkel, R., M. A. Goldin, J. A. Smith, O. M. Sun, A. A. Aja, M. N. Bui, and T. Hughen, 2011: The Wirewalker: A vertically profiling instrument carrier powered by ocean waves. *J. Atmos. Oceanic Technol.*, **28**, 426–435, https://doi.org/10.1175/2010JTECHO805.1.

Polzin, K. L., 2025: Covariance based estimates of near-boundary diapycnal upwelling in a submarine canyon. arXiv, 2508.05679, https://doi.org/10.48550/arXiv.2508.05679.

——, and Y. V. Lvov, 2011: Toward regional characterizations of the oceanic internal wavefield. *Rev. Geophys.*, **49**, RG4003, https://doi.org/10.1029/2010RG000329.

——, and T. J. McDougall, 2022: Mixing at the ocean's bottom boundary. *Ocean Mixing*, Elsevier, 145–180.

——, J. M. Toole, and R. W. Schmitt, 1995: Finescale parameterizations of turbulent dissipation. *J. Phys. Oceanogr.*, **25**, 306–328, https://doi.org/10.1175/1520-0485(1995)025<0306:FPOTD>2.0.CO;2.

——, ——, J. R. Ledwell, and R. W. Schmitt, 1997: Spatial variability of turbulent mixing in the abyssal ocean. *Science*, **276**, 93–96, https://doi.org/10.1126/science.276.5309.93.

——, B. Wang, Z. Wang, F. Thwaites, and A. J. Williams, 2021: Moored flux and dissipation estimates from the northern deepwater Gulf of Mexico. *Fluids*, **6**, 237, https://doi.org/10.3390/fluids6070237.

Qiu, B., S. Chen, J. Wang, and L.-L. Fu, 2024: Seasonal and fortnight variations in internal solitary waves in the Indonesian seas from the SWOT measurements. *J. Geophys. Res. Oceans*, **129**, e2024JC021086, https://doi.org/10.1029/2024JC021086.

Raja, K. J., M. C. Buijsman, J. F. Shriver, B. K. Arbic, and O. Siyanbola, 2022: Near-inertial wave energetics modulated by background flows in a global model simulation. *J. Phys. Oceanogr.*, **52**, 823–840, https://doi.org/10.1175/JPO-D-21-0130.1.

——, ——, A. Bozec, R. W. Helber, J. F. Shriver, A. Wallcraft, E. P. Chassignet, and B. K. Arbic, 2024: Spurious internal wave generation during data assimilation in eddy resolving ocean model simulations. *Ocean Modell.*, **188**, 102340, https://doi.org/10.1016/j.ocemod.2024.102340.

Ramadhan, A., and Coauthors, 2020: Oceananigans.jl: Fast and friendly geophysical fluid dynamics on GPUs. *J. Open Source Software*, **5**, 2018, https://doi.org/10.21105/joss.02018.

Ray, R. D., and G. T. Mitchum, 1996: Surface manifestation of internal tides generated near Hawaii. *Geophys. Res. Lett.*, **23**, 2101–2104, https://doi.org/10.1029/96GL02050.

Rocha, C. B., T. K. Chereskin, S. T. Gille, and D. Menemenlis, 2016: Mesoscale to submesoscale wavenumber spectra in Drake Passage. *J. Phys. Oceanogr.*, **46**, 601–620, https://doi.org/10.1175/JPO-D-15-0087.1.

Rumelhart, D. E., G. E. Hinton, and R. J. Williams, 1986: Learning representations by back-propagating errors. *Nature*, **323**, 533–536, https://doi.org/10.1038/323533a0.

Sanford, T. B., 1971: Motionally induced electric and magnetic fields in the sea. *J. Geophys. Res.*, **76**, 3476–3492, https://doi.org/10.1029/JC076i015p03476.

——, J. H. Dunlap, J. A. Carlson, D. C. Webb, and J. B. Girton, 2005: Autonomous velocity and density profiler: EM-APEX. *Proc. IEEE/OES Eighth Working Conf. on Current Measurement Technology*, Southampton, United Kingdom, Institute of Electrical and Electronics Engineers, 152–156, https://doi.org/10.1109/CCM.2005.1506361.

Santos-Ferreira, A. M., and Coauthors, 2025: The Internal Waves Service Workshop: Observing internal waves globally with deep learning and synthetic aperture radar. *Bull. Amer. Meteor. Soc.*, **106**, E1462–E1470, https://doi.org/10.1175/BAMS-D-25-0133.1.

Savage, A. C., and Coauthors, 2017: Spectral decomposition of internal gravity wave sea surface height in global models. *J. Geophys. Res. Oceans*, **122**, 7803–7821, https://doi.org/10.1002/2017JC013009.

Schönau, M. C., and Coauthors, 2025: How do tides affect underwater acoustic propagation? A collaborative approach to improve internal wave modeling at basin to global scales. *Oceanography*, **8** (2), 24–35, https://doi.org/10.5670/oceanog.2025.308.

Shchepetkin, A. F., and J. C. McWilliams, 2005: The Regional Oceanic Modeling System (ROMS): A split-explicit, free-surface, topography-following-coordinate oceanic model. *Ocean Modell.*, **9**, 347–404, https://doi.org/10.1016/j.ocemod.2004.08.002.

Simmons, H. L., and M. H. Alford, 2012: Simulating the long-range swell of internal waves generated by ocean storms. *Oceanography*, **25** (2), 30–41, https://doi.org/10.5670/oceanog.2012.39.

——, R. W. Hallberg, and B. K. Arbic, 2004: Internal wave generation in a global baroclinic tide model. *Deep-Sea Res. II*, **51**, 3043–3068, https://doi.org/10.1016/j.dsr2.2004.09.015.

Sinnett, G., K. A. Davis, A. J. Lucas, S. N. Giddings, E. Reid, M. E. Harvey, and I. Stokes, 2020: Distributed temperature sensing for oceanographic applications. *J. Atmos. Oceanic Technol.*, **37**, 1987–1997, https://doi.org/10.1175/JTECH-D-20-0066.1.

Siyanbola, O. Q., M. C. Buijsman, A. Delpech, L. Renault, R. Barkan, J. F. Shriver, B. K. Arbic, and J. C. McWilliams, 2023: Remote internal wave forcing of regional ocean simulations near the U.S. West Coast. *Ocean Modell.*, **181**, 102154, https://doi.org/10.1016/j.ocemod.2022.102154.

——, ——, ——, R. Barkan, Y. Pan, and B. K. Arbic, 2024: Interactions of remotely generated internal tides with the U.S. West Coast continental margin. *J. Geophys. Res. Oceans*, **129**, e2023JC020859, https://doi.org/10.1029/2023JC020859.

Skitka, J., B. K. Arbic, Y. Ma, K. Momeni, Y. Pan, W. R. Peltier, D. Menemenlis, and R. Thakur, 2024a: Internal-wave dissipation mechanisms and vertical structure in a high-resolution regional ocean model. *Geophys. Res. Lett.*, **51**, e2023GL108039, https://doi.org/10.1029/2023GL108039.

——, ——, R. Thakur, D. Menemenlis, W. R. Peltier, Y. Pan, K. Momeni, and Y. Ma, 2024b: Probing the nonlinear interactions of supertidal internal waves using a high-resolution regional ocean model. *J. Phys. Oceanogr.*, **54**, 399–425, https://doi.org/10.1175/JPO-D-22-0236.1.

Spence, D., O. Kitzler, C. Taylor, S. Curtis, B. Neimann, J. Dawes, J. Downes, and H. Pask, 2024: Depth-resolved water temperature measurements using Raman lidar. *Appl. Opt.*, **63**, 4366–4371, https://doi.org/10.1364/AO.524112.

Srinivasan, A., T. M. Chin, E. P. Chassignet, M. Iskandarani, and N. Groves, 2022: A statistical interpolation code for ocean analysis and forecasting. *J. Atmos. Oceanic Technol.*, **39**, 367–386, https://doi.org/10.1175/JTECH-D-21-0033.1.

Sun, B., Z. Jing, M. Yuan, H. Yang, and L. Wu, 2024: Effects of horizontal resolution on long-range equatorward radiation of near-inertial internal waves in ocean general circulation models. *J. Adv. Model. Earth Syst.*, **16**, e2024MS004216, https://doi.org/10.1029/2024MS004216.

Sun, S., R. Bleck, C. G. Rooth, J. Dukowicz, E. P. Chassignet, and P. Killworth, 1999: Inclusion of thermobaricity in isopycnic-coordinate ocean models. *J. Phys. Oceanogr.*, **29**, 2719–2729, https://doi.org/10.1175/1520-0485(1999)029<2719:IOTIIC>2.0.CO;2.

SWOT, 2024a: SWOT level 2 KaRIn low rate sea surface height data product version C. NASA Physical Oceanography Distributed Active Archive Center, accessed 1 June 2025, https://doi.org/10.5067/SWOT-SSH-2.0.

——, 2024b: SWOT postlaunch oceanography field campaign L2 moorings Ver. 1. NASA Physical Oceanography Distributed Active Archive Center, accessed 1 February 2025, https://doi.org/10.5067/SWTPO-MOOR2.

Tchonang, B., and Coauthors, 2026: SWOT geostrophic velocity validation against in-situ measurements in the California current. *Earth Space Sci.*, in press.

Thakur, R., and Coauthors, 2022: Impact of vertical mixing parameterizations on internal gravity wave spectra in regional ocean models. *Geophys. Res. Lett.*, **49**, e2022GL099614, https://doi.org/10.1029/2022GL099614.

Varma, D., M. Buijsman, O. Q. Siyanbola, M. Andres, A. F. Waterhouse, and U. Send, 2026: A multivariable plane-wave fit technique to extract unidirectional internal wave fluxes from an internal wave resolving mooring array. ESS Open Archive, https://doi.org/10.22541/essoar.176832457.75358854/v1.

Villamaña, M., and Coauthors, 2017: Role of internal waves on mixing, nutrient supply and phytoplankton community structure during spring and neap tides in the upwelling ecosystem of Ría de Vigo (NW Iberian Peninsula). *Limnol. Oceanogr.*, **62**, 1014–1030, https://doi.org/10.1002/lno.10482.

Wagner, G. L., and Coauthors, 2025: High-level, high-resolution ocean modeling at all scales with Oceananigans. arXiv, 2502.14148v2, https://doi.org/10.48550/arXiv.2502.14148.

Wang, J., and Coauthors, 2022: On the development of SWOT in situ calibration/validation for short-wavelength ocean topography. *J. Atmos. Oceanic Technol.*, **39**, 595–617, https://doi.org/10.1175/JTECH-D-21-0039.1.

——, and Coauthors, 2025: SWOT mission validation of sea surface height measurements at sub-100 km scales. *Geophys. Res. Lett.*, **52**, e2025GL114936, https://doi.org/10.1029/2025GL114936.

Waterhouse, A. F., and Coauthors, 2014: Global patterns of diapycnal mixing from measurements of the turbulent dissipation rate. *J. Phys. Oceanogr.*, **44**, 1854–1872, https://doi.org/10.1175/JPO-D-13-0104.1.

Weaver, A. T., 2003: 3D-Var and 4D-Var approaches to ocean data assimilation. *ECMWF Workshop on the Role of the Upper Ocean in Medium and Extended Range Forecasting*, Shinfield Park, Reading, ECMWF, 57–66, https://www.ecmwf.int/en/elibrary/76865-3d-var-and-4d-var-approaches-ocean-data-assimilation.

Whalen, C. B., L. D. Talley, and J. A. MacKinnon, 2012: Spatial and temporal variability of global ocean mixing inferred from Argo profiles. *Geophys. Res. Lett.*, **39**, L18612, https://doi.org/10.1029/2012GL053196.

White, L., and A. J. Adcroft, 2008: A high-order finite volume remapping scheme for nonuniform grids: The Piecewise Quartic Method (PQM). *J. Comp. Phys.*, **227**, 7394–7422, https://doi.org/10.1016/j.jcp.2008.04.026.

——, ——, and R. W. Hallberg, 2009: High-order regridding–remapping schemes for continuous isopycnal and generalized coordinates in ocean models. *J. Comput. Phys.*, **228**, 8665–8692, https://doi.org/10.1016/j.jcp.2009.08.016.

Whitley, V., and J. Wenegrat, 2025: Breaking internal waves on sloping topography: Connecting parcel displacements to overturn size, interior-boundary exchanges, and mixing. *J. Phys. Oceanogr.*, **55**, 645–661, https://doi.org/10.1175/JPO-D-24-0052.1.

Whitwell, C. A., N. L. Jones, G. N. Ivey, M. G. Rosevear, and M. D. Rayson, 2024: Ocean mixing in a shelf sea driven by energetic internal waves. *J. Geophys. Res. Oceans*, **129**, e2023JC019704, https://doi.org/10.1029/2023JC019704.

Wunsch, C., and R. Ferrari, 2004: Vertical mixing, energy, and the general circulation of the oceans. *Annu. Rev. Fluid Mech.*, **36**, 281–314, https://doi.org/10.1146/annurev.fluid.36.050802.122121.

Xu, C., and E. D. Zaron, 2024: Detecting instantaneous tidal signals in ocean models utilizing streaming band-pass filters. *J. Adv. Model. Earth Syst.*, **16**, e2024MS004319, https://doi.org/10.1029/2024MS004319.

——, and ——, 2025: Parameterization of frequency-dependent internal wave drag in global ocean models. *J. Adv. Model. Earth Syst.*, **17**, e2025MS005126, https://doi.org/10.1029/2025MS005126.

Xu, X., E. P. Chassignet, A. J. Wallcraft, B. K. Arbic, M. C. Buijsman, and M. Solano, 2022: On the spatial variability of the mesoscale sea surface height wavenumber spectra in the Atlantic Ocean. *J. Geophys. Res. Oceans*, **127**, e2022JC018769, https://doi.org/10.1029/2022JC018769.

Yadidya, B., 2023: Replication data for: "Phase-accurate internal tides in a global ocean forecast model: Potential applications for nadir and wide-swath altimetry". Harvard Dataverse, accessed 10 November 2023, https://doi.org/10.7910/DVN/HMDTRZ.

——, B. K. Arbic, J. F. Shriver, A. D. Nelson, E. D. Zaron, M. C. Buijsman, and R. Thakur, 2024: Phase-accurate internal tides in a global ocean forecast model: Potential applications for nadir and wide-swath altimetry. *Geophys. Res. Lett.*, **51**, e2023GL107232, https://doi.org/10.1029/2023GL107232.

——, ——, ——, E. D. Zaron, M. C. Buijsman, L. Carrère, M. Tchilibou, and T. Uchida, 2025a: Advancing internal tide correction for SWOT Cal/Val: The role of ocean forecasts. *Earth Space Sci.*, **12**, e2025EA004511, https://doi.org/10.1029/2025EA004511.

——, J. F. Shriver, and B. K. Arbic, 2025b: Internal tide SSH corrections for SWOT Cal/Val from a HYCOM forecast system. Harvard Dataverse, accessed 31 October 2025, https://doi.org/10.7910/DVN/QQUQNZ.

Zaron, E. D., 2019: Baroclinic tidal sea level from exact-repeat mission altimetry. *J. Phys. Oceanogr.*, **49**, 193–210, https://doi.org/10.1175/JPO-D-18-0127.1.

——, and R. D. Ray, 2023: Clarifying the distinction between steric and baroclinic sea surface height. *J. Phys. Oceanogr.*, **53**, 2591–2596, https://doi.org/10.1175/JPO-D-23-0073.1.

Zeiden, K., J. Thomson, A. Shcherbina, and E. D'Asaro, 2024: Observations of elevated mixing and periodic structures within diurnal warm layers. *J. Geophys. Res. Oceans*, **129**, e2024JC021399, https://doi.org/10.1029/2024JC021399.

Zhang, X., X. Li, and Q. Zheng, 2021: A machine-learning model for forecasting internal wave propagation in the Andaman Sea. *IEEE J. Sel. Top. Appl. Earth Obs. Remote Sens.*, **14**, 3095–3106, https://doi.org/10.1109/JSTARS.2021.3063529.

Zhao, Z., M. Alford, J. Girton, L. Rainville, and H. Simmons, 2016: Global observations of open-ocean mode-1 M_2 internal tides. *J. Phys. Oceanogr.*, **46**, 1657–1684, https://doi.org/10.1175/JPO-D-15-0105.1.

Zulberti, A., N. L. Jones, and G. N. Ivey, 2020: Observations of enhanced sediment transport by nonlinear internal waves. *Geophys. Res. Lett.*, **47**, e2020GL088499, https://doi.org/10.1029/2020GL088499.